Precision Measurement Using Cavity Optomechanics

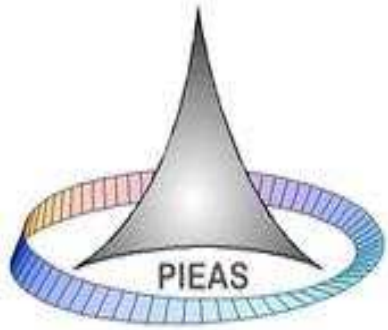

Asad Mehmood

2021

Department of Physics and Applied Mathematics
Pakistan Institute of Engineering and Applied Sciences,
Nilore, Islamabad, Pakistan

This page intentionally left blank

Reviewers and Examiners

Foreign Reviewers

1. Prof. Dr. Barry C. Sanders

Institute of Quantum Science and Technology, University of Calgary.

2. Prof. Dr. Mauro Paternostro

School of Mathematics and Physics, Queens University Belfast.

Thesis Examiners

1. Prof. Dr. Aslam Baig

National Center for Physics, Quaid-e-Azam University, Islamabad.

2. Dr. Muhammad Nawaz

Chief Scientist (Retd.), National Institute of Lasers and Optronics, Nilore, Islamabad.

3. Prof. Dr. Abdul Hameed Toor

Department of Physics, Quaid-e-Azam University, Islamabad.

Head of Department(Name): Prof. Dr. Muhammad Aftab Rafiq

Signature with Date: _____

Certificate of Approval

This is to certify that research work presented in this thesis titled as **Precision Measurement Using Cavity Optomechanics**, was conducted by **Mr. Asad Mehmood**, under the supervision of **Dr. Shahid Qamar**.

No part of this thesis has been submitted anywhere else for any other degree. This thesis is submitted to the department of **Physics and Applied Mathematics** in partial fulfillment of the requirements for the degree of **Doctor of Philosophy** in the field of **Physics**.

Student Name: **Asad Mehmood** Signature: _____

Examination committee:

Examiners	**Name, Designation & Address**	**Signature**
Internal Examiner 1		
Internal Examiner 2		
Supervisor	Prof. Dr. Shahid Qamar, Director, Center of Mathematical Sciences, PIEAS, Islamabad	
Head of Department	Prof. Dr. Muhammad Aftab Rafiq, Head, Department of Physics and Applied Mathematics, PIEAS, Islamabad	
Dean Research PIEAS	Prof. Dr. Naeem Iqbal, Dean Research, PIEAS, Islamabad	

Thesis Submission Approval

This is to certify that the work contained in this thesis entitled **Precision Measurement Using Cavity Optomechanics**, was carried out by **Asad Mehmood**, and in my opinion, it is fully adequate, in scope and quality, for the degree of **Ph.D.** Furthermore, it is hereby approved for submission for review and thesis defense.

Supervisor: _____

Name: **Dr. Shahid Qamar**

Date:

Place: PIEAS, Islamabad.

Head, Department of Physics
and Applied Mathematics: _____

Name: **Dr. M. Aftab Rafiq**

Date:

Place: PIEAS, Islamabad.

Precision Measurement Using Cavity Optomechanics

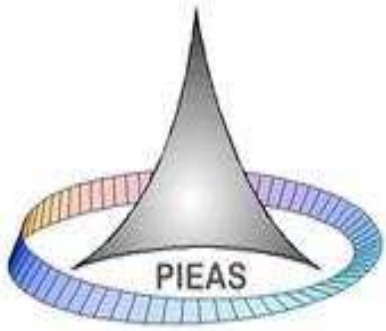

Asad Mehmood

Submitted in partial fulfillment of the requirements
for the degree of Ph.D.
April, 2021

Department of Physics and Applied Mathematics
Pakistan Institute of Engineering and Applied Sciences,
Nilore, Islamabad, Pakistan

Dedications

To my parents, wife and son

Author's Declaration

I, **Asad Mehmood** hereby declare that my Ph.D. thesis titled **Precision Measurement Using Cavity Optomechanics**, is my own work and has not been submitted previously by me or anybody else for taking any degree from Pakistan Institute of Engineering and Applied Sciences (PIEAS) or any other university / institute in the country / world.

At any time if my statement is found to be incorrect (even after my graduation), the university has the right to withdraw my Ph.D. degree.

Name: **Asad Mehmood**

Date:

Place: PIEAS, Islamabad.

Plagiarism Undertaking

I, **Asad Mehmood** solemnly declare that research work presented in the thesis titled **Precision Measurement Using Cavity Optomechanics**, is solely my research work with no significant contribution from any other person. Small contribution / help wherever taken has been duly acknowledged or referred and that complete thesis has been written by me.

I understand the zero tolerance policy of the HEC and Pakistan Institute of Engineering and Applied Sciences (PIEAS) towards plagiarism. Therefore, I as an author of the thesis titled above declare that no portion of my thesis has been plagiarized and any material used as reference is properly referred / cited.

I undertake that if I am found guilty of any formal plagiarism in the thesis titled above even after the award of my Ph.D. degree, PIEAS reserves the rights to withdraw / revoke my Ph.D. degree and that HEC and PIEAS has the right to publish my name on the HEC / PIEAS Website on which name of students are placed who submitted plagiarized thesis.

Name: **Asad Mehmood**

Date:

Place: PIEAS, Islamabad.

Acknowledgements

First of all, I am very thankful to Almighty ALLAH for all his blessings and giving me the ability to complete this research work.

I am thankful to my supervisor Dr. Shahid Qamar for being a great mentor throughout this period and helping with ideas and encouragement during hard times.

Higher Education Commission of Pakistan deserves thanks for providing funds for this research work under Indigenous Ph.D. scholarship scheme (PIN#315-719-2PS3-005). Interaction with the HEC administrative staff at different times has always been very helpful.

I would also like to express my sincere gratitude to my senior office colleagues Dr. Abdul Ghani Akram, Mr. Shamsuddin and Mr. Muhammad Rustam for their support and facilitation in various matters during my PhD.

I am also thankful to my friends, Dr. Rizwan Ahmad, Dr. Mirqad Ayaz, Dr. Nisar Ahmad, Dr. Muhammad Waqas, Mr. Anees Ahmad, Mr. Muhammad Saddique, Mr. Saifullah, Mr. Muhammad Bilal Iqbal, Mr. Shafiq-ur-Rehman and Mr. Rabnawaz Khan for their fruitful discussions, facilitation and encouragement during my research work.

Finally, I am greatly indebted to my beloved parents and wife for their prayers and encouragement, because without their love and support this work might have not been completed. I would also like to mention my little boy Muhammad Ali Hassanain for putting smile on my face in frustrating times.

(Asad Mehmood)

PIEAS, Islamabad.

Copyrights Statement

Table of Contents

List of Figures

Abstract

Optomechanical (OM) system is formed by an optical or microwave cavity containing a movable mechanical element that can support collective oscillational modes. It is a rapidly growing field showing great potential in precision measurement of small displacements, forces, electrical charges, and magnetic fields.

The coupling between light and mechanical element in OM system could be dispersive, dissipative or both at the same time. Dispersive coupling results in position dependence of the cavity eigen-modes while in dissipative coupling the cavity linewidth is position dependent. Detection of weak classical forces via dispersive coupling has a long history. However, recent studies show that dissipative coupling can also allow force sensing beyond the standard quantum limit (SQL).

In this thesis, we have mainly focused on the detection of weak classical force using dissipatively coupled OM system. First, we study the effects of laser phase noise (LPN) associated with the cavity drive on the detection of a weak force on a free test mass. Our results show that for an optimum choice of various parameters, one can realize force sensing below SQL even in the presence of LPN.

The analysis is further extended by introducing a parametric amplifier (PA) in the system and driving it with a noisy pump. The presence of PA improves force sensitivity much better than SQL. However, LPN associated with PA pump strongly affects force sensing. Interestingly, we find that for an optimum choice of different parameters, force sensitivity better than SQL can still be realized.

We also investigate the effects of Kerr medium on force sensing of an OM oscillator. Our analysis show that the presence of Kerr medium improves force sensing beyond SQL. Moreover, increasing the strength of Kerr non-linearity not only improves force sensitivity but also increases the measurement bandwidth. Kerr medium also leads to the robustness of the system against thermal fluctuations.

In our final theoretical proposal, we present an optical detection technique based on dissipative OM coupling for the detection of weak magnetic field. Our analysis suggest measurement of magnetic field upto sub-nano-Tesla level at room temperature while working in the bad-cavity regime.

List of Publications

This thesis is based on the first four of the following publications:

Journal Publications

1. **Asad Mehmood**, Sajid Qamar, and Shahid Qamar, "Effects of laser phase fluctuation on force sensing for a free particle in a dissipative optomechanical system ", Phys. Rev. A, vol. 98, p 053841, 2018.

2. **Asad Mehmood**, Sajid Qamar, and Shahid Qamar, "Force sensing in a dissipative optomechanical system in the presence of parametric amplifier's pump phase noise", Phys. Scr., vol. 94, p 095502, 2019.

3. **Asad Mehmood**, Sajid Qamar, and Shahid Qamar, "Measuring weak magnetic field via dissipatively coupled opto-mechanical system", Phys. Scr., vol. 95, p 035102, 2020.

4. **Asad Mehmood**, Sajid Qamar, and Shahid Qamar, "Effects of Kerr medium on force sensing in a dissipative optomechanical system", EPL, vol. 131, p 24005, 2020.

5. **Asad Mehmood**, Muhammad Saddique, Sajid Qamar, and Shahid Qamar, "Effects of finite bandwidth on atomic grating in a three level ladder type system", Optics Communications, vol 472, p 125881, 2020.

List of Abbreviations and Symbols

MO	Mechanical Oscillator
OM	Optomechanical
FPI	Fabry-Pérot Interferometer
MSI	Michelson-Sagnac Interferometer
RWA	Rotating Wave Approximation
PA	Parametric Amplifier
SQL	Standard Quantum Limit
LPN	Laser Phase Noise
ω_m	Frequency of Mechanical Mode
G	Parametric Gain
η	Dissipative Coupling Constant
ω_c	Frequency of Optical Mode
ω_l	Input Laser Frequency
κ	Cavity Decay Rate
γ_m	Mechanical Damping Rate
$\mathbb{P}$	Input Laser Power
Δ	Detuning
ξ	Brownian Noise Operator
Γ_L	Laser Linewidth
K_B	Boltzmann Constant

Chapter 1

Introduction

1.1 Brief History of Optomechanics

Radiation pressure results from the transfer of momentum from light to a solid object upon reflection, absorption or emission. The concept of radiation pressure was first introduced by J. Kepler in 1619 in order to explain why the tail of a comet always points away from the Sun. In 1873, J. C. Maxwell introduced his electromagnetic theory in the form of Maxwell equations which also predicted the fact that light carries momentum [1]. Later in 1900, a Russian physicist Prof. P. N. Lebedev for the first time experimentally demonstrated the effects of radiation pressure on material objects [2]. His experiment verified with high confidence that for electromagnetic radiation of power $\mathbb{P}$ at normal incidence, the associated momentum can be written as $p = \frac{\mathbb{P}}{c}(1+\rho)$, where ρ is the reflectivity of the illuminated surface and c is the speed of light. In an independent experimental work, E. F. Nichols and G. F. Hull in 1901 also measured radiation pressure [3].

It may be noted that radiation pressure force associated with light is extremely faint. For instance, 1 watt laser at normal incidence on a perfectly reflecting mirror exerts approximately 6 nN of force. This is the reason, why it took so long to observe the mechanical effects of light in laboratory. However, technological advancements during past few decades have made it possible to study and maneuver the mechanical effects of light which eventually opened new avenues in the field of physics.

An optical cavity with a mechanical oscillator can be coupled to radiation pressure force to form an optomechanical (OM) device [4–6]. These devices are

rich in the context of observing and controlling the mechanical effects of light and lead to the study of various novel effects like cooling of mechanical oscillator to its quantum-mechanical ground state [7–10], generation of slow light [11–13], quantum state transfer [14–17], gravitational wave interferometery [18–20] and many more [21, 22]. The size of OM systems range from nanometer/femtogram scale for on-chip phononic and photonic crystals to kilometer/kilogram scale of large Michelson interferometer for the detection of gravitational waves.

Optomechanics also brings about the interesting idea of observing quantum effects on macroscopic scale. For example, *entanglement* which is a characteristic trait associated with quantum systems can be observed between macroscopic oscillator and optical field of the cavity. The idea was theoretically proposed by Vitali et al. [23] and also observed experimentally by Palomaki et al [24].

The field of optomechanics emerged due to the development of early gravitational wave detectors in late 1970s. Quantum mechanics entered into the picture when it was realized that the measurement of position of the end mirrors of the interferometer cannot be made with arbitrary precision. Rather, vacuum fluctuations of the optical field set a limit on sensitivity of position measurements. Therefore, it could also result in mechanical oscillations on quantum scale [25–30].

1.2 Precision Measurement via Optomechanics

Early research in OM systems was primarily based on the detection of gravitational waves. However, as the research continued, soon it was realized that OM systems have great potential in precision measurement. Since then OM systems advanced the art of precision measurement. Measurement of small displacement [31–35], force [36–44], torque [45], electrical charge [46], magnetic field [47–49] can be made with remarkable sensitivity.

1.2.1 Force Sensing

The coupling between the optical and mechanical degrees of freedom in optomechanical systems could be dispersive, dissipative or both at the same time. In dispersively coupled OM systems, displacement of the mechanical oscillator (MO)

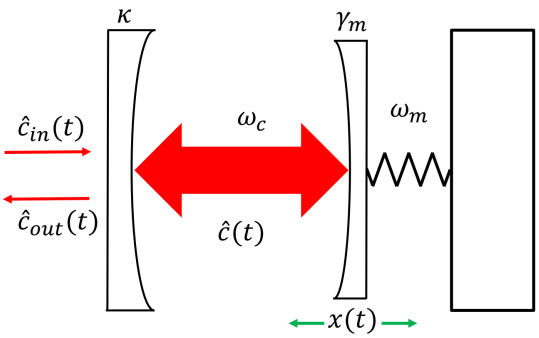

Figure 1.1: Schematics of a Fabry-Pérot cavity with a fixed and movable mirror. Here ω_m and γ_m represent frequency and damping of MO respectively while ω_c and κ represent frequency of the cavity and optical decay rate, respectively.

modulates the eigen-modes of the optical cavity. A simple example of dispersive coupling is a standard Fabry-Pérot interferometer (FPI) with one movable mirror that provides an additional mechanical degree of freedom as shown in Fig. (1.1).

The detection of a weak classical force using dispersive OM system to reduce quantum noise and surpass the standard quantum limit (SQL) has a long history. For instance, it has been shown that the force sensitivity can be improved by using a squeezed vacuum [27,40,50]. In another scheme, the idea of OM speed meter was proposed to monitor clasical force on a test mass which results in measurement sensitivity better than SQL [36, 39]. In an interesting study, it was shown that the use of Kerr cell in interferometric gravity-wave detector counters the radiation pressure induced fluctuations. The performance of such interferometers greatly surpass SQL [51]. It may be noted that SQL fundamentally arises due to the Heisenberg uncertainty principle. By definition, SQL of a measurement error is the limit mean square value of the estimate for one observable calculated from the measurement results of its conjugate observable [52].

A lot of work has been done in dispersively coupled OM system, however, it has its own constraints e.g. requirement of side-band resolved regime for ground state cooling [7, 8] which is not always feasible particularly in the case of low mechanical frequencies. However, such requirements are not necessary for dissipatively coupled OM cavities [53–57].

In dissipative coupling, the displacement of the mechanical oscillator modulates the decay rate of the optical cavity. The dissipation in this case does not lead to

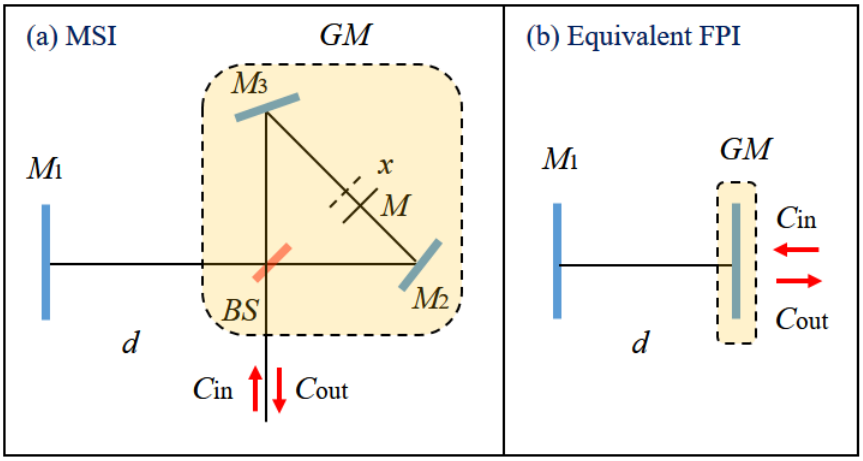

Figure 1.2: (a) Michelson Sagnac Interferometer (as a generalize mirror GM) works as an input mirror of the Fabry-Pérot cavity. (b) The effective Fabry-Pérot cavity.

decoherence or absorption of light, rather it results in loss-less coupling between a continuous optical wave and a mode of the optical cavity. This coupling enables the optical cavity to perform as a perfect transducer.

The idea of dissipative coupling was first proposed theoretically by Elste et al [53] and studied in different systems [45, 54, 55, 57–60]. Dissipatively coupled OM systems enables ground state cooling of mechanical oscillators without requiring the resolved-side-band condition [53–57, 59–62]. There are a variety of interesting physical effects which were discussed with dissipative coupling for example, the normal mode splitting [56, 60, 61], electromagnetically induced transparency [56, 60], and the squeezing of the output light [63, 64]. Various optomechanical systems were studied for dissipative coupling based on Febry-Pérot Interferometer [45, 58–60] and Michelson-Sagnac Interferometer (MSI) [54, 55, 57] among many others. In a recent study, it was also shown that purely dissipative coupling in a bad cavity regime results in strong reduction of the backaction and suppression of the squeezing ability of the system [65]. A practical realization is shown in Fig. (1.2) based on MSI with a movable membrane M which acts as a compound mirror (GM) [54, 55, 57]. The position of M and transmission of the beam splitter BS sensitively affects the overall transmission of GM. The compound mirror GM along with a perfect mirror M_1 forms an effective FPI whose linewidth now sensitively depends upon the position of the membrane.

1.2.2 Force Sensing via Dissipatively Coupled System

In a recent study, it was shown that the dissipative coupling in an OM system can be used for the measurement of a classical force on a free particle having sensitivity better than the Standard Quantum Limit (SQL) [42]. Moreover, the sensitivity of a classical force on a free particle was found to be comparable with that of the dispersive OM system, however, it has a much wider measurement bandwidth. The idea of force measurement in a dissipative system was further extended with the use of parameteric amplifier (PA) [43]. It was shown that the presence of PA allows much better force sensitivity (surpassing the SQL) over a wide range of detection frequencies even in the presence of mechanical damping and thermal noise. It was also shown that an increase in the parametric gain reduces the effects of mechanical damping and thermal noise. The presence of PA also makes the system more robust against thermal noise.

1.2.3 Effects of Laser Phase Noise (LPN) on Force Sensing

The optical field of a single mode laser oscillating far above threshold is in a state that is very close to the coherent state. The intensity of the field is almost free from fluctuations due to intrinsic saturation, however, the phase of the field fluctuates randomly in time. If we perform successive measurements, the state of the field appears to be a mixture of coherent states.

Typically, the effects of phase noise associated with the laser are ignored. However, it has profound impact on many applications for example, entanglement generation in a correlated spontaneous emission laser (CEL) is highly sensitive to the phase fluctuation [66, 67]. Moreover, ground state cooling and OM entanglement are strongly affected by LPN [68–70].

The spectral density of a laser operating far above threshold, can be approximated well by a Lorentzian function [71, 72]. However, by taking a Lorentzian line shape overestimate the effects of LPN. For instance, in an earlier study by Diósi [73], a white noise model was proposed for LPN which suggested no possibility of ground state cooling contrary to the experimental findings of low phonon numbers. Later, a more realistic model was proposed by Rabl et al. [74], which

suggest the experimental feasibility of optical ground-state cooling and coherent operations in OM systems. Following the same approach as discussed in Ref. [74] for noise model, we assume $\phi(t)$ to be a zero mean Gaussian noise process, the correlation function can be written as

$$\{\dot{\phi}(s)\dot{\phi}(s')\} = \int \frac{d\omega}{2\pi} S_{\dot{\phi}}(\omega) e^{-i\omega(s-s')}, \tag{1.1}$$

where $\{\}$ represents average over different noise values. For each experimental setup the frequency noise spectrum $S_{\dot{\phi}}(\omega)$ is specific. In our case the noise spectrum is given as [74]

$$S_{\dot{\phi}}(\omega) = \frac{2\Gamma_l}{1 + \omega^2/\gamma_c^2}, \tag{1.2}$$

where Γ_l represents the laser linewidth and γ_c^{-1} represents the finite correlation time of the LPN. In the limiting case of $\gamma_c \to \infty$, white noise model is recovered.

In this thesis, we incorporate LPN in dissipatively coupled OM system and investigate its effects on force measurement. First we consider the system presented in Ref. [42] for dissipative coupling and introduce LPN associated with the laser that drives the system. The effects of LPN are investigated, our results show that LPN strongly affects the sensitivity of force measurement [75]. Next, we consider dissipatively coupled system with a parametric amplifier (PA) as discussed in Ref. [43]. We introduce LPN in the drive laser of PA and investigate its effects on force sensing. In this case again, LNP strongly affects the measurement sensitivity [76]. Detailed analysis is presented in Chapter 2 and Chapter 3.

1.2.4 Effects of Kerr Medium on Force Sensing

The presence of Kerr cell in an optical cavity results in a nonlinear phase shift which is proportional to the intensity of light [77]. The effects of Kerr cell has been studied in the context of quantum-non-demolition (QND) measurement of photon number operator [78, 79]. It has also been shown that use of Kerr cell in an interferometric gravity-wave-detector counters the radiation pressure induced fluctuations which results in performance of such interferometer greatly surpassing SQL [51]. The presence of strong Kerr non-linearity inside an optical cavity also in-

hibits normal mode splitting (NMS) due to photon blockade mechanism [80]. The increase in Kerr nonlinearity results in progressive decreases in NMS. Therefore, Kerr medium can be used to coherently control the micro-mirror's dynamics. Kerr medium can also enhance stationary entanglement in OM system [81]. Another interesting feature which can be observed in OM cavity in the presence of Kerr medium is optical bistability of intracavity intensity [82]. This effect can be used in design and development of all-optical switches and high sensitivity sensors [83].

In view of all these interesting features of Kerr medium in OM systems, we have studied its effects on force sensing using a dissipative OM system. For dissipative OM system, we have considered the system proposed by Vyatchanin et al. [42]. We then introduced an optical Kerr media inside the cavity and studied its effects on force sensing capability of a MO. The presence of Kerr media not only improved the measurement sensitivity below SQL but also made the system more robust against the thermal noise. A detailed analysis is presented in Chapter 4.

1.2.5 Magnetic Field Sensing via Dissipatively Coupled System

The precision measurement of weak magnetic field has gained a lot of interest due to its practical application in various fields like geology, material characterization and medicine [84]. Magnetometers based on superconducting quantum interference devices (SQUID) operating at cryogenic temperatures, magnetostrictive magnetometers and atomic magnetometers provides remarkable sensitivity [85–89]. In recent studies, the magnetic field sensors based on OM cavity were also proposed, they have small size, high sensitivity and operational capability at room temperature [47, 49]. In another study, a technique based on optomechanical induced transparency (OMIT) was proposed for the detection of weak magnetic fields [48].

In this thesis, we also present an optical detection technique for measuring weak magnetic field which can work at room temperature. We use a dissipatively coupled OM system that can be realized in a Michelson-Sagnac interferometer (MSI) with a movable membrane [53–55] as shown in Fig. (1.2). The transmissivity of this system when operating close to the dark port condition, sensitively depends

upon the position of the movable mirror/membrane. Thus, the linewidth of the cavity sensitively depends upon the position of the membrane. When current is applied to the membrane in the presence of magnetic field, the position of the membrane changes which in turn changes the linewidth of the cavity. Therefore, by observing the spectrum of the output field, magnetic field upto sub-nano-Tesla levels can be measured. Detail of the scheme is presented in Chapter 5.

1.3 Thesis Structure

The contents of the rest of this thesis are divided into five chapters.

Chapter 2: Focuses on the effects of laser phase noise (LPN) on the detection of a weak classical force that acts on a free particle in a dissipative optomechanical (OM) system. In this chapter, the effect of mechanical damping and thermal noise on force sensing in the presence of LPN have also been investigated.

Chapter 3: The presence of PA in a dissipatively coupled OM system improves force sensitivity much better than the standard quantum limit (SQL) over a wider range of detection frequency [43]. This chapter deals with the effects of LPN associated with the pump laser that drives the parametric amplifier (PA). The effects of LPN on force sensing on a free test mass have been discussed here.

Chapter 4: Optical Kerr medium has the ability to transform amplitude fluctuations in the initial coherent state into phase fluctuations [90] and therefore can result in the improvement of the detection of weak force. In this chapter, the effects of Kerr medium on the detection of a weak classical force acting on an OM oscillator have been discussed in dissipatively coupled OM system. The influence of Kerr medium on thermal fluctuations has also been considered in this chapter.

Chapter 5: An optical detection technique is proposed for the detection of weak magnetic field which is based on dissipatively coupled OM system. Our proposal suggests measurement of weak magnetic field upto sub-nano-Tesla levels at room temperature.

Chapter 6: In this chapter, we summarize all of our results in detail and conclude the thesis.

Chapter 2

Effects of Laser Phase Fluctuation on Force Sensing in a Dissipatively Coupled Optomechanical System

2.1 Introduction

Dissipatively coupled optomechanical (OM) systems have gained considerable attention due to its ability of cooling the mechanical oscillator to its ground state without requiring the good cavity regime [53]. Later, it was also considered for normal mode splitting [60,91], optomechanical induced transparency [60] and squeezing of the output light [63]. The dissipative coupling has been demonstrated experimentally for several interesting systems like silicon nitride membrane in a cavity-enhanced Michelson-Sagnac interferometer for optomechanical cooling [55], photonic crystal split-beam nanocavity for the detection of nanoscale sources of torque [45] and others. In a recent study, it was shown that dissipative coupling in an optomechanical systems can be used for the measurement of a classical force on a free mass having sensitivity better than the Standard Quantum Limit (SQL) [42]. Moreover, the sensitivity of a classical force on a free mass was found to be comparable with that of the dispersive OM system however, it has a much wider measurement bandwidth.

In this chapter, we study the effects of laser phase noise (LPN) on the detection of a weak classical force that acts on a free mass in a dissipatively coupled OM system [42, 54]. We also investigate the effect of mechanical damping and thermal noise on force measurement in the presence of LPN. Typically, the effects of phase noise associated with the laser are ignored. However, it has profound

impact on many applications for example, the effects of LPN has been studied for entanglement generation in a correlated spontaneous emission laser (CEL) and it was found that entanglement generation is highly sensitive to the phase fluctuation [66, 67]. Ground state cooling and OM entanglement in presence of LPN was also considered in some earlier studies [68–70]. They have discussed the feasibility of ground state cooling in OM systems and the strong effects of LPN on OM entanglement.

In section 2.2, we present our model and solve the equations of motion using quantum Langevin equation formalism. In section 2.3, we find an expression for the output quadrature of the field and calculate the noise spectral density. In section 2.4, we study the effect of mechanical damping and thermal noise on the force sensitivity in the presence of phase fluctuation. In section 2.5 we summarize our results.

2.2 Theory and Model

We consider an optomechanical system in which a free mass m is dissipatively coupled to a cavity field with eigenfrequency ω_o [42, 92]. For the realization of dissipative coupling, we consider a system which is based on a Michelson-Sagnac Interferometer (MSI) as proposed by Xuereb et al. [54] as shown in Fig. (1.2). The schematic diagram shows an interferometer that contains a generalized input mirror GM which itself is an interferometer and provides the necessary dissipative coupling for the Fabry-Perot interferometer. The mirror M_1 is perfectly reflecting and d is the distance between the beam splitter and the end mirror. Under the assumption that the size of GM is much smaller than d, the reflectance and transmittance of GM are constant without having any dependence on spectral frequency. The GM demonstrates pure dissipative coupling because the spatial shift of M changes only the relaxation rate of the cavity and not its eigenfrequency. This feature of MSI is discussed in detail in Ref. [42,54]. The movable mirror M can be considered as a free mass at the time scale much smaller than the oscillation period. For a free particle, potential energy is zero, its momentum and kinetic energy are conserved. The cavity is pumped resonantly with a strong coherent

light of frequency $\omega_p = \omega_o$. We assume that the pump laser has phase fluctuation $\phi(t) = \int \dot{\phi}(t')dt'$ with zero mean value. The Hamiltonian of the system is given by

$$\begin{aligned} \hat{H} &= \hbar\omega_o c^\dagger c + \frac{p^2}{2m} + \int \hbar\omega b^\dagger(\omega) b(\omega) d\omega \\ &- i\hbar\sqrt{\kappa}\left[c^\dagger c_{in} e^{-i[\omega_p t + \phi(t)]} - c_{in}^\dagger c e^{i[\omega_p t + \phi(t)]}\right]. \end{aligned} \tag{2.1}$$

Here $\kappa = \kappa_o(1 + \eta x)$ represents the position dependent photon decay rate, κ_o is the decay rate for $x = 0$ and $\eta = \kappa_{cp}/\kappa_o$, where κ_{cp} is the dissipative coupling constant between the cavity field and the free particle. The first term represents the free energy of the cavity field, the second term represents the energy of the free particle, the third term represents the bosonic bath and the fourth term represents the cavity-bath interaction which gives attenuation of the pump photons and associated quantum noise. In order to incorporate the effects of LPN associated with the drive laser, we follow the noise model of Rabl et al. [74] as discussed in section (1.2.3).

In the presence of an external weak force F_{ex} acting on the free mass with zero mean value the Heisenberg's equations of motion for the system are given by

$$\dot{x} = \frac{p}{m}, \tag{2.2a}$$

$$\dot{p} = \frac{i\hbar\eta\sqrt{\kappa_o}}{2}[c^\dagger c_{in} e^{-i[\omega_p t + \phi(t)]} - c_{in}^\dagger c e^{i[\omega_p t + \phi(t)]}] + F_{ex}, \tag{2.2b}$$

$$\dot{c} = -(\frac{\kappa}{2} + i\omega_o)c + \sqrt{\kappa} c_{in} e^{-i(\omega_p + \dot{\phi})t}. \tag{2.2c}$$

The output field of the system can equally be obtained by the input output formalism [90] and is given by

$$c_{out} = -c_{in} + \sqrt{\kappa} c, \tag{2.3}$$

with the frame rotating at the instantaneously fluctuating frequency $(\omega_p + \dot{\phi})$ Eqs. (2.2a)-(2.2c) takes the following form:

$$\dot{c} = -(\frac{\kappa}{2} - i\dot{\phi})c + \sqrt{\kappa}c_{in}, \tag{2.4a}$$

$$\ddot{x} = \frac{\dot{p}}{m} = \frac{i\hbar\eta\sqrt{\kappa}_o}{2m}[c^\dagger c_{in} - c_{in}^\dagger c] + \frac{F_{ex}}{m}. \tag{2.4b}$$

These operators can be represented as a sum of large mean value and small fluctuating terms such that $c = \overline{c} + \delta c, c_{in} = \overline{c}_{in} + \delta c_{in}, c_{out} = \overline{c}_{out} + \delta c_{out}, p = \overline{p} + \delta p, x = \overline{x} + \delta x$, where

$$\delta c_{in} = -\int b(\omega)e^{-i(\omega-\omega_p)t}\frac{d\omega}{2\pi}, \tag{2.5}$$

represents the fluctuating part of the input drive and the corresponding correlations are defined as

$$\left[b(\omega),\ b^\dagger(\omega')\right] = 2\pi\delta(\omega - \omega'), \tag{2.6a}$$

$$\left[\delta c_{in}(t),\ \delta c_{in}^\dagger(t')\right] = \delta(t - t'). \tag{2.6b}$$

We assume the steady-state displacement of the free particle to be $\overline{x} = 0$. In steady state, $\dot{x} = 0$, $\dot{p} = m\ddot{x} = 0$ and $\dot{c} = 0$, under this condition Eqs. (2.4a) and (2.4b) lead to the solution $\overline{p} = 0$, $\overline{c} = (2/\sqrt{k_o})\overline{c}_{in}$, $\overline{c}_{out} = \overline{c}_{in}$. We also assume the input field to be real i.e., $\overline{c}_{in} = \overline{c}_{in}^* = \sqrt{\mathbb{P}/\hbar\omega_l}$, where $\mathbb{P}$ is the power of input field. In the first order approximation, we obtain the linearized equations of motion for fluctuating operators such that

$$\delta\dot{c} = -\frac{\kappa}{2}\delta c - \frac{\eta\kappa_o\overline{c}}{4}x + \sqrt{\kappa_o}\delta c_{in} + i\dot{\phi}\overline{c}, \tag{2.7a}$$

$$\delta c_{out} = -\delta c_{in} + \sqrt{\kappa_o}\delta c + \frac{\eta\sqrt{\kappa_o}\overline{c}}{2}x, \tag{2.7b}$$

$$\ddot{x} = \frac{i\hbar\eta\sqrt{\kappa}_o}{2m}[(\delta c_{in} - \delta c_{in}^\dagger) - \frac{\kappa_o}{2}(\delta c - \delta c^\dagger)] + \frac{F_{ex}}{m}. \tag{2.7c}$$

In frequency domain these equations can be written as

$$\delta c_{out+} = \left(\frac{\kappa_o + 2i\omega}{\kappa_o - 2i\omega}\right) b_+ - \frac{\eta\sqrt{\kappa_o}\bar{c}}{\kappa_o - 2i\omega} i\omega x_\omega + \frac{2i\sqrt{\kappa_o}\bar{c}}{\kappa_o - 2i\omega}\dot{\phi}_+, \tag{2.8a}$$

$$x_\omega = -\frac{\hbar\eta\bar{c}\sqrt{\kappa_o}}{m\omega^2\left(\kappa_o - 2i\omega\right)}\left[\omega\left(b_+ - b_-^\dagger\right) + \frac{\bar{c}\sqrt{\kappa_o}}{2}\left(\dot{\phi}_+ + \dot{\phi}_-\right)\right] - \frac{f_{ex}}{m\omega^2}. \tag{2.8b}$$

where $\dot{\phi}_\pm = \dot{\phi}(\omega_o \pm \omega)$ represents the Fourier amplitude of the corresponding operator.

It is interesting to note that in the presence of LPN, the output field given by Eq. (2.8a) still carries the information about the speed $i\omega x_\omega$ of the probe mass in frequency domain. However, an additional term due to LPN also appears in this case. Similarly, the probe's displacement equation given by Eq. (2.8b) also carries an additional noise term due to LPN.

2.3 Detection of Classical Force in the Presence of Laser Phase Noise

Next we consider the detection of classical force acting on the free test mass in the presence of phase fluctuations associated with the laser driving the system. In order to do that we write the input and output fields in terms of their amplitude and phase quadrature. Thus, $A_{in} = (b_+ + b_-^\dagger)/\sqrt{2}$ and $p_{in} = (b_+ - b_-^\dagger)/i\sqrt{2}$ represent the amplitude and phase quadratures of input field while $A_{out} = (\delta c_{out+} + \delta c_{out-}^\dagger)/\sqrt{2}$ and $p_{out} = (\delta c_{out+} - \delta c_{out-}^\dagger)/i\sqrt{2}$ represent amplitude and phase quadratures of the output field. The input quadratures are related with $b_+(b_-^\dagger)$ while output quadratures are related with $\delta c_{out+}(\delta c_{out-}^\dagger)$. By using Eqs. (2.8a) and (2.8b), we obtain following expressions for the quadratures of the output filed:

$$\begin{aligned} A_{out} = \left(\frac{\kappa_o + 2i\omega}{\kappa_o - 2i\omega}\right)\Bigg[A_{in} - \frac{2\hbar\eta^2\bar{c}^2}{m\left(\kappa_o^2 + 4\omega^2\right)}p_{in} + \frac{i\sqrt{2\kappa_o}\eta\bar{c}}{\kappa_o + 2i\omega}\frac{f_{ex}}{m\omega} \\ + \frac{i\sqrt{2\kappa_o}\bar{c}}{\kappa_o + 2i\omega}\left(\dot{\phi}_+ - \dot{\phi}_-\right) + \frac{i\sqrt{2\kappa_o}\hbar\eta^2\bar{c}^3\kappa_o}{2m\omega\left(\kappa_o^2 + 4\omega^2\right)}\left(\dot{\phi}_+ + \dot{\phi}_-\right)\Bigg], \end{aligned} \tag{2.9a}$$

$$p_{out} = \left(\frac{\kappa_o + 2i\omega}{\kappa_o - 2i\omega}\right)\left[p_{in} + \frac{\sqrt{2\kappa_o}\bar{c}}{\kappa_o - 2i\omega}\left(\dot{\phi}_+ + \dot{\phi}_-\right)\right]. \tag{2.9b}$$

In order to write the above equations in much simplified form, we define following parameters:

$$
\begin{aligned}
&Q = \frac{P\kappa_o^2}{\kappa_o^2 + 4\omega^2},\ P = \frac{2\hbar\eta^2\bar{c}^2}{m\kappa_o},\ F_{SQL} = \sqrt{2\hbar m\omega^2},\\
&f_s = e^{i\beta}\frac{f_{ex}}{F_{SQL}},\ e^{i\beta} = i\frac{\kappa_0 - 2i\omega}{\sqrt{\kappa_o^2 + 4\omega^2}},\\
&M_1 = \frac{\sqrt{2\kappa_o}Q}{4\omega} - ie^{i\beta}\sqrt{\frac{2Q}{\kappa_o P}},\ M_2 = \frac{\sqrt{2\kappa_o}Q}{4\omega} + ie^{i\beta}\sqrt{\frac{2Q}{\kappa_o P}}
\end{aligned}
\tag{2.10}
$$

Here P is the dimensionless power parameter and is related to the input power as $\mathbb{P} = \frac{m\kappa_o^2\omega_l}{8\eta^2}P$ and f_s represents the signal force normalized to SQL of force F_{SQL}. By using the above mentioned parameters, the output quadrature given by Eqs. (2.9a) and (2.9b) can be written in a much simplified form as given by the following relations:

$$
A_{out} = \left(\frac{\kappa_o + 2i\omega}{\kappa_o - 2i\omega}\right)\left[A_{in} - Qp_{in} + \sqrt{2Q}f_s + i\bar{c}\left(M_1\dot{\phi}_+ + M_2\dot{\phi}_-\right)\right], \tag{2.11a}
$$

$$
p_{out} = \left(\frac{\kappa_o + 2i\omega}{\kappa_o - 2i\omega}\right)\left[p_{in} + \bar{c}\left(\frac{M_1 - M_2}{2}\right)\left(\dot{\phi}_+ + \dot{\phi}_-\right)\right]. \tag{2.11b}
$$

It is clear from Eq. (2.11a) that the amplitude quadrature of the output field contains shot noise (1st term), back action (2nd term), force signal (3rd term) and the LPN term (4th term). While the phase quadrature of the output field given by Eq. (2.11b) has information regarding input phase quadrature (1st term) and LPN (2nd term). It is also clear from Eqs. (2.11a) and (2.11b) that our results reduces to the same results as discussed in Ref. [42] in the absence of LPN. It is also interesting to note that in the limit $2\omega/\kappa_o << 1$ (i.e., the bad cavity regime) and in the absence of LPN and external force, Eqs. (2.11a) and (2.11b) reduce to $A_{out} \approx A_{in} + \sqrt{P}[\frac{1}{2}(2\omega/\kappa_o)^2 - 1]p_{in}$ and $p_{out} = p_{in}$. The reduction in back action is evident in the amplitude quadrature. This feature of MSI tuned at pure dissipative coupling regime has been discussed in detail in Ref. [65].

In order to achieve optimum detection strategy, it is better to define a generalized output field quadrature such that

$$
\delta Z = A_{out}\cos\theta + p_{out}\sin\theta, \tag{2.12}
$$

where θ represents the reference phase in homodyne detection that can be optimized to achieve better sensitivity. It may be pointed out that the local oscillator is produced by splitting off a part of the input laser, as a result, it also contains the laser phase noise. In order to incorporate its effects, we follow the same approach as discussed by Abdi et al., [69] and consider all the detected quantities in a frame rotating at randomly fluctuating instantaneous frequency i.e., $(\omega_o + \dot{\phi})$. The correlation function for $\delta\tilde{c}_{in}(t) \rightarrow \delta c_{in}(t)e^{i\omega_o t + i\phi(t)}$ in the rotating frame is still given by Eq. (2.6b).

On substituting output quadratures from Eqs. (2.11a) and (2.11b) in Eq. (2.12), we obtain our generalized output quadrature in terms of fluctuating input field quadratures ($A_{in},\ p_{in}$), fluctuating phase ($\dot{\phi}_{\pm}$) and SQL normalized signal force (f_s). The fluctuating input field quadratures and fluctuating phase terms in the generalized output quadrature represents the Fourier component of noise and is found to be

$$\begin{aligned} f_N &= \frac{e^{-i\beta}}{\sqrt{2}}\left[\frac{A_{in}}{\sqrt{Q}} + \left(-\sqrt{Q} + \frac{\tan\theta}{\sqrt{Q}}\right)p_{in}\right. \\ &+ \left. i\bar{c}\left\{\frac{2M_1 + i(M_2 - M_1)\tan\theta}{\sqrt{Q}}\dot{\phi}_+ + \frac{2M_2 + i(M_2 - M_1)\tan\theta}{\sqrt{Q}}\dot{\phi}_-\right\}\right]. \end{aligned} \tag{2.13}$$

When $f_N < f_s$, the force signal is detectable and when $f_s = 1$, the signal is at SQL [40]. It is interesting to note that the homodyne angle θ can be optimized to eliminate the back action term completely from the noise spectrum [93–97]. This can be done by taking

$$\tan\theta_{opt} = \frac{P\kappa_o^2}{\kappa_o^2 + 4\omega_o^2}. \tag{2.14}$$

The single-sided spectral density of noise can be calculated by using the standard relation [40]

$$\frac{1}{2}2\pi S_N(\omega)\delta(\omega - \omega') = \frac{1}{2}\big[\langle f_N(\omega)f_N^{\dagger}(\omega')\rangle + \langle f_N^{\dagger}(\omega')f_N(\omega)\rangle\big], \tag{2.15}$$

assuming the spectral densities of the input field quadratures to be $S_{A_{in}} = S_{p_{in}} = 1$ with no cross-correlation i.e, $S_{A_{in}p_{in}} = 0$ and for the laser phase fluctuation we use

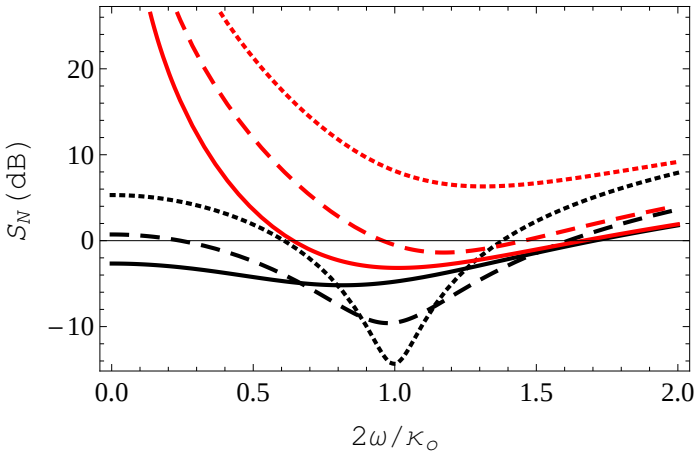

Figure 2.1: Here light shaded lines show noise spectrum in the presence of phase fluctuations while dark shaded lines show the case of no phase fluctuation. The horizontal line corresponds to SQL. Here solid , dashed and dotted lines correspond to $P = 3, 9$ and 27, respectively. Here $m = 100$ ng, $\kappa_o = 2\pi$ MHz, $\eta = 4.182 \times 10^8$ m^{-1}, $\Gamma_l = 10$ Hz, $\gamma_c = 200$ Hz.

Eq. (1.2). The noise spectral density is found to be

$$S_N = \frac{1}{2}\left[\frac{1}{Q} + \left(-\sqrt{Q} + \frac{\tan\theta}{\sqrt{Q}}\right)^2 + \frac{2\Gamma_l}{1+\omega^2/\gamma_c^2}\bar{c}^2\left\{\frac{\kappa_o Q}{4\omega^2} + \frac{4}{\kappa_o P}(1+\tan^2\theta) - 4\sqrt{\frac{Q}{P(\kappa_o^2+4\omega^2)}}\tan\theta\right\}\right]. \tag{2.16}$$

From Eq. (2.16) it is clear that by selecting the optimum homodyne angle according to Eq. (2.14), the back action term can be eliminated completely.

Next, we present the results of our numerical simulation. It may be noted that throughout our calculations, we use $m = 100$ ng, $\kappa_o = 2\pi$ MHz, $\lambda = 1064$ nm and $\eta = 4.182 \times 10^8$ m^{-1} which are the same as discussed in Ref. [43]. Figure (2.1) shows a comparison of noise spectrum S_N in the absence and presence of laser phase noise. The dark shaded lines correspond to the case when there is no phase fluctuation while the light shaded lines correspond to situation when the effects of phase fluctuation are incorporated into the system. The dotted lines, dashed lines and solid lines correspond to power parameter $P = 27$, 9, 3 respectively. Other parameters are $\Gamma_l = 10$ Hz and $\gamma_c = 200$ Hz. It is interesting to see that SQL can still be achieved for a wide range of detection frequencies even in the presence

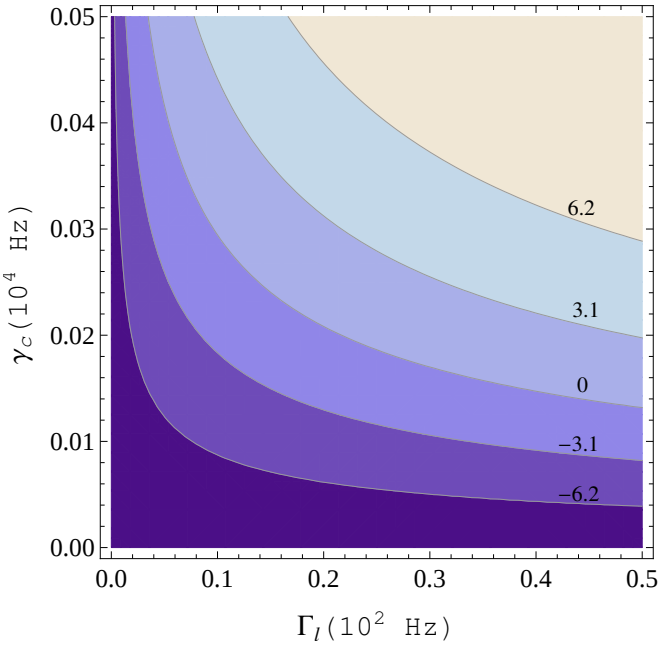

Figure 2.2: Contour plot of noise spectrum S_N against laser linewidth Γ_l and noise correlation parameter γ_c. Here the line at $S_N = 0$ dB corresponds to SQL and the region below this line gives better than SQL sensitivity. Here the power parameter $P = 6$ and all the other parameters are the same as in Fig. 2.1.

of laser phase noise provided the power levels are kept low as clearly shown by light shaded continuous and dashed lines. To get an insight of this situation, we consider the noise spectrum S_N given by Eq. (2.16) which contains a shot noise term, back-action term and laser phase noise term. For an optimum angle at $2\omega/\kappa_o = 1$, Eq. (2.14) reduces to $\tan\theta_{opt} = P/2 = Q$ which results in complete elimination of the back-action from the noise spectrum. The braces $\{\}$ term in Eq. (2.16), which is related to the phase noise, reduces to $(1/2\kappa_o)[P+8/P]$, which shows clear dependence of phase noise on the input power P. The phase noise increases in both cases i.e., when power level is either very large or very small. However, there exists an intermediate power range in which below SQL sensitivity can be achieved. That is why, we have both upper and lower bound on the power levels (See also Fig. (2.3)).

In figure (2.2) we present a contour plot which shows the effect of laser linewidth and finite correlation time on noise spectrum. The contour at $S_N = 0$ dB represents SQL. The positive values of the contour correspond to above SQL and negative values of the contour correspond to below SQL. It is clear from the re-

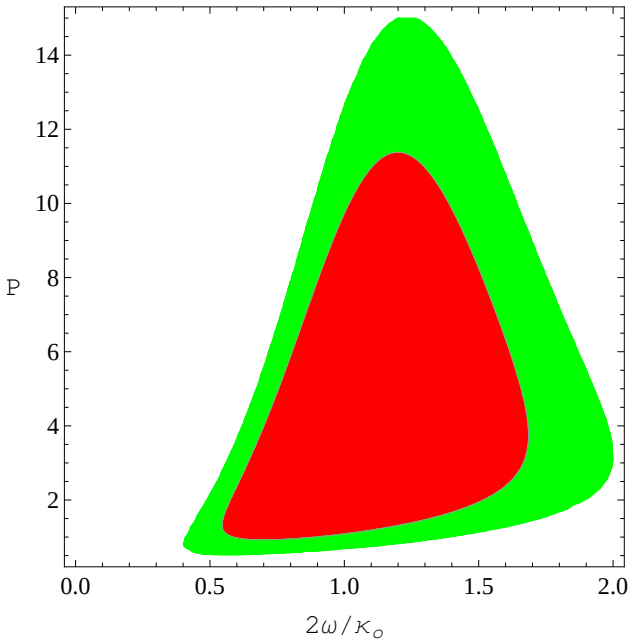

Figure 2.3: Contour plot of noise spectrum S_N against P and $2\omega/\kappa_o$. The dark shaded region (in red) corresponds to below SQL sensitivity. Here $\Gamma_l = 10$ Hz and $\gamma_c = 200$ Hz. All the other parameters are the same as in Fig. 2.1.

sults that the laser linewidth and the correlation time must be selected in a manner to remain in the negative portion of the contour to obtain below SQL measurement. The contour is plotted at the optimum homodyne phase value of $2\omega/\kappa_o = 1$ for power parameter $P = 6$.

In order to get further insight, next we show contour plot of noise spectrum against the input power parameter P and the detection frequency $2\omega/\kappa_o$ (See Fig. (2.3)). Only the dark shaded region in Fig. (2.3) corresponds to below SQL sensitivity. Here the laser linewidth and noise correlation parameter are considered to be $\Gamma_l = 10$ Hz and $\gamma_c = 200$ Hz, respectively. It is clear from the contour plot that the power levels for which below SQL sensitivity can be achieved range from 0.95 to 11.5. Thus for higher power level force sensitivity below SQL cannot be achieved. This is also evident from Fig. 2.1 (where the light dotted line is at power level of 27).

2.4 Force Detection on Free Mass in the Presence of Phase Fluctuations, Damping and Thermal Noise

In this section, we consider the effect of mechanical damping of the free particle and its interaction with the thermal environment in presence of LPN. The equations of motion in this case are as follows

$$\dot{c} = -(\frac{\kappa}{2} - i\dot{\phi})c + \sqrt{\kappa}c_{in}, \tag{2.17a}$$

$$\ddot{x} = \frac{i\hbar\eta\sqrt{\kappa_o}}{2m}[c^\dagger c_{in} - c_{in}^\dagger c] - \frac{\gamma_m p}{m} + \frac{\xi}{m} + \frac{F_{ex}}{m}. \tag{2.17b}$$

Here γ_m represents the mechanical damping rate and ξ is the thermal noise coupling of the free particle with zero mean value. In this case, the displacement of the free particle and the output field in frequency domain evolve in the following way:

$$\delta c_{out+} = \left(\frac{\kappa_o + 2i\omega}{\kappa_o - 2i\omega}\right)\left[b_+ - \frac{\eta\sqrt{\kappa_o}\bar{c}}{\kappa_o + 2i\omega} i\omega x_\omega + \frac{2i\sqrt{\kappa_o}\bar{c}}{\kappa_o + 2i\omega}\dot{\phi}_+\right], \tag{2.18a}$$

$$\begin{aligned} x_\omega = &-\frac{\hbar\eta\bar{c}\sqrt{\kappa_o}}{m(\omega + i\gamma_m)(\kappa_o - 2i\omega)}\left(b_+ - b_-^\dagger\right) \\ &- \frac{\hbar\eta\bar{c}^2\kappa_o}{2m\omega(\omega + i\gamma_m)(\kappa_o - 2i\omega)}\left(\dot{\phi}_+ + \dot{\phi}_-\right) - \frac{f_{ex} + \xi}{m\omega(\omega + i\gamma_m)}. \end{aligned} \tag{2.18b}$$

Following the same procedure as we did in section 2.3, the amplitude and phase quadratures of the output field can be written as

$$A_{out} = \left(\frac{\kappa_o + 2i\omega}{\kappa_o - 2i\omega}\right)\left[A_{in} - \frac{Q}{B}p_{in} + \frac{\sqrt{2Q}}{B}\frac{f_{ex} + \xi}{F_{SQL}}e^{i\beta} + i\bar{c}\left(M_1'\dot{\phi}_+ + M_2'\dot{\phi}_-\right)\right], \tag{2.19a}$$

$$p_{out} = \left(\frac{\kappa_o + 2i\omega}{\kappa_o - 2i\omega}\right)\left[p_{in} + \bar{c}B\left(\frac{M_1' - M_2'}{2}\right)\left(\dot{\phi}_+ + \dot{\phi}_-\right)\right], \tag{2.19b}$$

where Q and P are the same parameters as defined in Eq. (2.10) while the parameter B, M_1' and M_2' are defined as

$$\begin{aligned} B &= (1 + i\gamma_m/\omega), \\ M_1' &= \frac{\sqrt{2\kappa_o}Q}{4\omega} - \frac{ie^{i\beta}}{B}\sqrt{\frac{2Q}{\kappa_o P}}, \\ M_2' &= \frac{\sqrt{2\kappa_o}Q}{4\omega} + \frac{ie^{i\beta}}{B}\sqrt{\frac{2Q}{\kappa_o P}}. \end{aligned} \tag{2.20}$$

For a generalized quadrature δZ as defined earlier, the noise f_N in this case is given by the following relation

$$\begin{aligned} f_N &= \frac{e^{-i\beta}}{\sqrt{2}} B\left[\frac{A_{in}}{\sqrt{Q}} + \left(-\frac{\sqrt{Q}}{B} + \frac{\tan\theta}{\sqrt{Q}}\right) p_{in} + \frac{\xi}{BF_{SQL}} e^{i\beta}\right. \\ &+ \left. i\bar{c}\left\{\frac{2M_1' + i(M_2' - M_1')B\tan\theta}{\sqrt{Q}}\dot{\phi}_+ + \frac{2M_2' + i(M_2' - M_1')B\tan\theta}{\sqrt{Q}}\dot{\phi}_-\right\}\right]. \end{aligned} \tag{2.21}$$

For random thermal force ξ, the correlation function is defined as

$$\langle \xi(\omega)\xi(\Omega)\rangle = 4\pi m K_B T \gamma_m \delta(\omega + \Omega) \tag{2.22}$$

and the corresponding noise spectrum can be written as $S_{th} = 4\pi m K_B T \gamma_m$, where K_B is the Boltzmann constant, T is the temperature of the environment and γ_m is the mechanical damping of the oscillator. The noise spectrum S_N in this case is given by the following:

$$\begin{aligned} S_N &= \frac{1}{2}\left[\frac{|B|^2}{Q} + \left\{Q + \frac{|B|^2}{Q}\tan^2\theta - (B + B^*)\tan\theta\right\} - \frac{8\pi m K_B T \gamma_m}{F_{SQL}^2}\right. \\ &+ \frac{2\Gamma_l}{(1 + \omega^2/\gamma_c^2)}\frac{|B|^2\bar{c}^2}{Q}\left\{\left(\frac{\sqrt{2\kappa_o}Q}{4\omega} - \sqrt{\frac{2Q}{\kappa_o P}}\left(\tan\theta\cos\beta - \frac{\sin(\beta - \delta)}{|B|}\right)\right)^2\right. \\ &+ \left(\sqrt{\frac{2Q}{\kappa_o P}}\left(\tan\theta\sin\beta + \frac{\cos(\beta - \delta)}{|B|}\right)\right)^2 \\ &+ \left(\frac{\sqrt{2\kappa_o}Q}{4\omega} - \sqrt{\frac{2Q}{\kappa_o P}}\left(\tan\theta\cos\beta + \frac{\sin(\beta - \delta)}{|B|}\right)\right)^2 \\ &+ \left.\left.\left(\sqrt{\frac{2Q}{\kappa_o P}}\left(\tan\theta\sin\beta - \frac{\cos(\beta - \delta)}{|B|}\right)\right)^2\right\}\right]. \end{aligned} \tag{2.23}$$

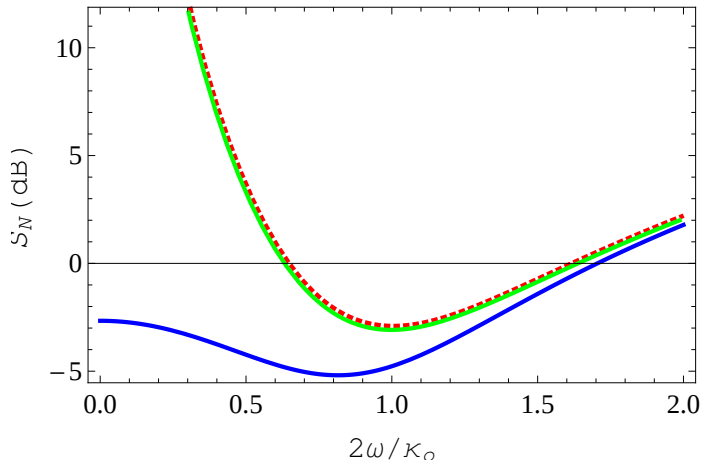

Figure 2.4: A comparison of noise spectrum: (dark solid line) without phase fluctuation, (light solid line) with phase fluctuation and (dotted line) with both damping and phase fluctuations. Here $P = 3$, $2\omega_o/\kappa_o = 1$, $\Gamma_l = 10$ Hz, $\gamma_c = 200$ Hz, $\gamma_m/\kappa_o = 10^{-5}$ and $T = 0$ K.

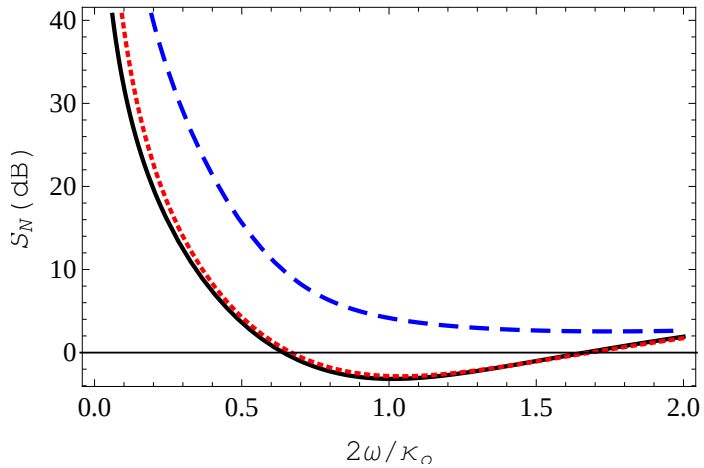

Figure 2.5: Effects of damping on noise spectrum: horizontal line refers to SQL, solid line corresponds to $\gamma_m/\kappa_o = 0$, dotted line corresponds to $\gamma_m/\kappa_o \simeq 0.1$ and the dashed line corresponds to $\gamma_m/\kappa_o \simeq 1$. All the other parameters are the same as in Fig. (2.4).

Here $|B| = \sqrt{1 + \omega^2/\gamma_m^2}$; $\beta = \tan^{-1}(\kappa_o/2\omega)$ and $\delta = \tan^{-1}(\gamma_m/\omega)$. In Eq. (2.23) the first term represents the photons shot noise, the second term corresponds to the radiation back pressure, third term gives the contribution of thermal noise and the last term corresponds to laser phase fluctuation noise. It may be noted that in the presence of mechanical damping, contribution from the radiation back action cannot be eliminated completely for any choice of optimum homodyne phase. However, minimum value of back action can be achieved by selecting the

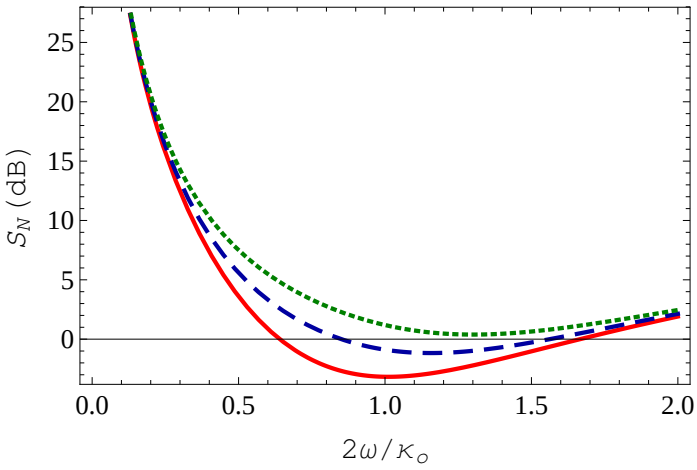

Figure 2.6: Effects of temperature on noise spectrum: solid, dashed and dotted lines correspond to $T = 0$ mK, 200 mK and 500 mK, respectively. Here $\gamma_m/\kappa_o = 10^{-5}$ and all the other parameters are the same as in Fig. (2.4).

homodyne phase θ such that

$$\tan\theta_{opt} = \frac{P\kappa_o^2}{(\kappa_o^2 + 4\omega^2)(1 + \gamma_m^2/\omega^2)}. \tag{2.24}$$

It may be noted that for $\gamma_m = 0$, this result reduces to Eq. (2.14).

Figure (2.4) shows a comparison of the noise spectrum in absence of phase fluctuation (dark solid line), with phase fluctuation (light solid line) and when both damping and phase fluctuation are present (dotted line). The temperature is taken to be at $T = 0$ K. Clearly there is no significant effect of damping on the noise spectrum for $\gamma_m/\kappa_o = 10^{-5}$. In order to further explore the effects of mechanical damping on noise spectrum consider Fig. (2.5) which shows the noise spectrum for different values of mechanical damping. It is clear that as long as $\gamma_m/\kappa_o << 1$, the effects of mechanical damping is negligible. However, when γ_m is of the order of κ_o, the noise spectrum is then significantly affected by mechanical damping as shown by the dashed line in Fig. (2.5).

Next we discuss the force sensitivity on the free particle when thermal fluctuations are also incorporated along with damping and phase fluctuations. Figure (2.6) shows the effects of finite temperature on noise spectrum. Here solid, dashed and dotted line corresponds to $T = 0$ mK, 200 mK and 500 mK, respectively. The mechanical damping is assumed to be $\gamma_m/\kappa_o = 10^{-5}$. It is clear that

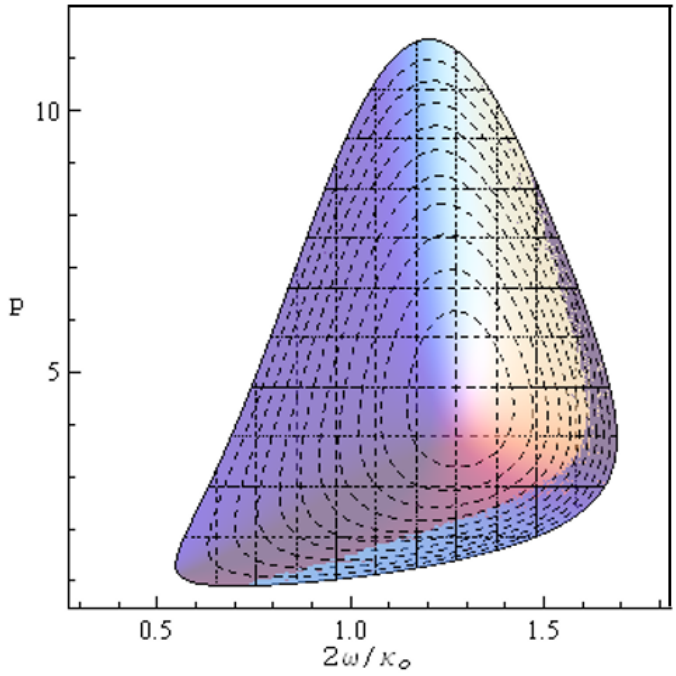

Figure 2.7: A Contour plot representing the force sensitivity as a function of $2\omega/\kappa_o$ and P. Here $\Gamma_l = 10$ Hz, $\gamma_c = 200$ Hz and $\gamma_m/\kappa_o = 10^{-5}$. The largest contour corresponds to $T = 0$ mK. By increasing the temperature the contours become smaller and vanishes for $T > 460$ mK, as a result no measurement at SQL is possible.

below SQL sensitivity can still be achieved in the presence of finite temperature however, force sensitivity decreases due to the increase in the temperature of the environment.

Figure (2.7) shows a contour plot of noise spectrum S_N against $2\omega/\kappa_o$ and P. The size of the contour decreases due to an increase in the temperature and eventually vanishes when T approaches 460 mK. In this figure the largest contour corresponds to $T = 0$ K and it spans input power range of $0.95 < P < 11.5$ while the allowed detection frequency range for this case is about $0.55 < 2\omega/\kappa_o < 1.68$. It is interesting to note that the largest contour in Fig. (2.7) which corresponds to $T = 0$ mK is almost similar to the contour shown in Fig. (2.3). The slight difference appears due to the non-zero value of mechanical damping.

2.5 Summary

In summary, our results show that the sensitivity of the force detection strongly depends upon the laser phase fluctuation. However, force measurement better than SQL can still be achieved with a wider frequency range for laser linewidth Γ_l of few tens of Hz and noise correlation parameter γ_c of few hundreds of Hz. We also considered the effect of mechanical damping and thermal noise in the presence of phase fluctuations. The mechanical damping doesn't affect the force measurement substantially as long as γ_m is much smaller than ω. Temperature of the environment greatly reduces the measurement sensitivity however, better then SQL measurement is still possible for temperature $T < 460$ mK if $\Gamma_l = 10$ Hz and $\gamma_c = 200$ Hz. In the presence of laser phase fluctuation and thermal noise, the magnitude of input power of the laser also influences the force measurement sensitivity. Our results show that below SQL measurement can neither be achieved for very low power levels nor for very high power levels. For laser power parameter $P < 0.95$, below SQL measurement is not possible while the upper level bound on power level P depends upon the value of Γ_l, γ_c and T. Thus an optimum choice of various parameters involved in the system play an important role for force measurement in the presence of LPN, damping and thermal noise.

Chapter 3

Force Sensing in a Dissipative Optomechanical System in the Presence of Parametric Amplifier's Pump Phase Noise

3.1 Introduction

The idea of dissipative coupling for the detection of weak force signal that acts on a free test mass was proposed by Vyatchanin et al. [42]. This scheme provides the possibility of detecting a classical force with sensitivity better than the SQL. The proposal was further extended with the introduction of a degenerate parametric amplifier (PA) into the system. It was shown that the presence of PA allows much better force sensitivity (as compared to the case when it is not present) even in the presence of mechanical damping and thermal noise [43]. In both of these studies, the effect of phase fluctuations associated with the driving laser field were ignored. In Chapter 2, we incorporated the phase fluctuation associated with the drive laser and thoroughly studied its effects on free mass force sensing in a dissipative OM system. It was shown that the sensitivity of force detection strongly depends upon LPN.

In this chapter, we study the effects of phase noise associated with the pump laser which drives the parametric amplifier (PA) on the detection of a weak classical force acting on a free test mass in a dissipative OM system. In order to incorporate the pump phase noise associated with PA in our system, we follow the noise model as proposed by Rabl et al. [74]. Our scheme can be realized by considering pure dissipative coupling setup based on a modified Michelson-Sagnac

interferometer [54]. The relative strength of the dispersive and dissipative coupling can be tuned so that the purely dissipative-coupling regime becomes experimentally feasible as demonstrated by Sawadsky et al. [55]. The parametric amplifier can be introduced in this setup with a separate pump as proposed by Ref. [62]. The paper is organized as follows. In section 3.2, we present our model and solve the equations of motion using quantum Langevin equation formalism. We find an expression for the output quadrature of the field and calculate the noise spectral density. In section 3.3, we present results of our numerical calculations. Finally, in section 3.4, we summarize our results.

3.2 Theory and Model

We consider an optomechanical (OM) system with a degenerate parametric amplifier PA [43, 62] where a free test mass m is dissipatively coupled to a cavity field with eigen-frequency ω_o. The potential energy of the free mass is zero and its momentum and kinetic energy are conserved. The cavity is driven resonantly with a strong coherent light of frequency $\omega_l = \omega_o$ and amplitude ε_l. A pump laser field of frequency $\omega_p = 2\omega_l$ interacts with the PA and produces an output field at frequency ω_l inside the cavity. We assume that the pump laser driving the PA has phase fluctuation $\phi(t) = \int \dot{\phi}(t')dt'$ with zero mean value. The Hamiltonian of the system in rotating frame at frequency ω_l is given by

$$\begin{aligned} \hat{H} &= \hbar(\omega_o - \omega_l)c^\dagger c + \frac{p^2}{2m} + i\hbar\sqrt{2\kappa}[\varepsilon_l(c^\dagger - c) \\ &+ c^\dagger c_{in} - c_{in}^\dagger c] + i\hbar G(c^{\dagger 2}e^{i\theta} - c^2 e^{-i\theta}), \end{aligned} \tag{3.1}$$

where $\kappa = \kappa_o(1 + \eta x)$ represents the position dependent photon decay rate and $\kappa = \kappa_o$ when $x = 0$. The parameter $\eta = \kappa_{cp}/\kappa_o$, where κ_{cp} is the dissipative coupling constant between the cavity field and the free test mass. The parameter θ is associated with the laser which drives PA and is given by $\theta = \theta_o + \phi(t)$, where θ_o is the reference phase and $\phi(t)$ is the fluctuating phase. The amplitude of the field is related to the input power as $\varepsilon_l = \sqrt{\mathbb{P}/\hbar\omega_l}$. The first term in the Hamiltonian represents the free energy of the cavity field, while the second term represents the energy of the free mass. The third term represents the coupling of

cavity field with the input laser and input vacuum noise represented by c_{in}. The last term represents the interaction between the cavity field and PA.

Here it may also be notted that, the cavity is driven with a laser of frequency ω_l while the PA is driven by a separate pump with frequency $\omega_p = 2\omega_l$. In practice, due to the power broadening in PA laser pump, the noise bandwidth associated with PA is much bigger than the laser that drives the cavity. Under this assumption, we can neglect the effects of the laser phase noise which drives the cavity against the effects of PA pump phase noise as discussed by Farman et al. [98]. For phase noise model, we follow the same approach as presented in section 1.2.3, in Chapter 1.

In the presence of an external weak force F_{ex} acting on the free mass with zero mean value, the Heisenberg equations of motion for the system are given by the following:

$$\dot{x} = \frac{p}{m}, \tag{3.2a}$$

$$\dot{p} = -\frac{i\hbar\eta\sqrt{2\kappa_o}}{2}[\varepsilon_l(c^\dagger - c) + c^\dagger c_{in} - c_{in}^\dagger c] + F_{ex}, \tag{3.2b}$$

$$\dot{c} = \sqrt{2\kappa_o}(1 + \frac{\eta}{2}x)(\varepsilon_l + c_{in}) + 2Gc^\dagger e^{i\theta} - \kappa_o(1 + \eta x)c. \tag{3.2c}$$

Here we assume that the steady-state displacement of the free particle to be zero i.e., $x_s = 0$. Under this condition the steady-state momentum and cavity field are found to be

$$p_s = 0,\ c_s = \frac{\sqrt{2\kappa_o}\varepsilon_l}{\kappa_o^2 - 4G^2}(\kappa_o + 2Ge^{i\theta_o}). \tag{3.3}$$

If we assume the deterministic part of the phase $\theta_o = 0$, the steady-state value of the cavity field becomes $c_s = \sqrt{2\kappa_o}\varepsilon_l(\kappa_o - 2G)^{-1}$, which is exactly the same as given in Ref [43] with the stability requirement of $\kappa_o > 2G$. The equations of motion for the operators given by Eqs. (3.2a)-(3.2c) can be represented as a sum of large mean value and small fluctuating terms such that $x = x_s + \delta x$, $p = p_s + \delta p$ and $c = c_s + \delta c$. In the first order approximation, the linearized equations of

motion are given by

$$\delta\dot{x} = \frac{\delta p}{m}, \tag{3.4a}$$

$$\delta\dot{p} = -\frac{i\hbar\eta\sqrt{2\kappa_o}}{2}[\varepsilon_l(\delta c^\dagger - \delta c) + c_s(c_{in} - c_{in}^\dagger)] + F_{ex}, \tag{3.4b}$$

$$\delta\dot{c} = -\kappa_o\delta c - (\kappa_o + 2G)\frac{c_s\eta\delta x}{2} + 2G(\delta c^\dagger + ic_s\phi) + \sqrt{2\kappa_o}c_{in}, \tag{3.4c}$$

By taking the Fourier transform of these operators, the cavity field and position fluctuation in frequency domain are found to be

$$\begin{aligned}\delta c(\omega) = \frac{1}{(\kappa_o - i\omega)^2 - 4G^2}\Bigg[&\sqrt{2\kappa_0}(\kappa_o - i\omega)c_{in}(\omega) \\ &+ 2G\sqrt{2\kappa_0}c_{in}^\dagger(-\omega) - (\kappa_o - i\omega + 2G)(\kappa_o + 2G) \\ &\times \frac{c_s\eta\delta x(\omega)}{2} - \frac{2Gc_s}{\omega}\Big\{(\kappa_o - i\omega)\dot{\phi}(\omega) - 2G\dot{\phi}(-\omega)\Big\}\Bigg],\end{aligned} \tag{3.5a}$$

$$\begin{aligned}\delta x(\omega) = &\frac{i\hbar\eta\sqrt{\kappa_o}c_s}{\sqrt{2}m\omega^2}\frac{4G - i\omega}{\kappa_o - i\omega + 2G}(c_{in} - c_{in}^\dagger) \\ &+ \frac{i\hbar\eta Gc_s^2}{m\omega^3}\frac{\kappa_o - 2G}{\kappa_o - i\omega + 2G}\Big[\dot{\phi}(\omega) + \dot{\phi}(-\omega)\Big] - \frac{f_{ex}}{m\omega^2}.\end{aligned} \tag{3.5b}$$

The output field of the system and its fluctuation can equally be obtained by the input output formalism [90] and are given by

$$c_{out} = -c_{in} + \sqrt{2\kappa}c, \tag{3.6a}$$

$$\delta c_{out}(\omega) = -c_{in}(\omega) + \sqrt{2\kappa_o}\delta c(\omega) + \sqrt{2\kappa_o}\frac{\eta c_s}{2}\delta x(\omega). \tag{3.6b}$$

On substituting Eqs. (3.5a) and (3.5b) in Eq. (3.6b), the fluctuating output field of the system is found to be

$$\begin{aligned}\delta c_{out}(\omega) \;=\; &-\frac{\sqrt{2\kappa_o}\eta c_s}{2}\frac{(4G + i\omega)}{\kappa_o - i\omega - 2G}\delta x(\omega) + \left[\frac{2\kappa_o(\kappa_o - i\omega)}{(\kappa_o - i\omega)^2 - 4G^2} - 1\right]c_{in}(\omega) \\ &+ \frac{4G\kappa_o}{(\kappa_o - i\omega)^2 - 4G^2}c_{in}^\dagger(\omega) - \frac{2c_sG\sqrt{2\kappa_o}\big[(\kappa_o - i\omega)\dot{\phi}(\omega) - 2G\dot{\phi}(-\omega)\big]}{\omega[(\kappa_o - i\omega)^2 - 4G^2]}.\end{aligned} \tag{3.7}$$

Equation (3.7), which is one of the main result of the paper clearly shows that the output field which contains information regarding the force signal and speed of the test mass depends upon the phase fluctuations associated with the laser driving

PA. Next, we define the input amplitude and phase quadratures as $X_{in}(\omega) = \frac{1}{\sqrt{2}}[c_{in}(\omega) + c_{in}^{\dagger}(-\omega)]$ and $Y_{in}(\omega) = \frac{1}{i\sqrt{2}}[c_{in}(\omega) - c_{in}^{\dagger}(-\omega)]$. Similarly, the output field's amplitude and phase quadratures are defined as $X_{out}(\omega) = \frac{1}{\sqrt{2}}[\delta c_{out}(\omega) + \delta c_{out}^{\dagger}(-\omega)]$ and $Y_{out}(\omega) = \frac{1}{i\sqrt{2}}[\delta c_{out}(\omega) - \delta c_{out}^{\dagger}(-\omega)]$. On substituting the values of $\delta c_{out}(\omega)$ and $\delta c_{out}^{\dagger}(\omega)$, the output quadratures of the field are found to be

$$X_{out} = \frac{\kappa_o + i\omega + 2G}{\kappa_o - i\omega - 2G}\Bigg[X_{in} + KY_{in} + \sqrt{2K}U\frac{f_{ex}(\omega)}{F_{SQL}(\omega)} - M_1\Big\{\dot{\phi}_+ - \dot{\phi}_-\Big\} - M_2\Big\{\dot{\phi}_+ + \dot{\phi}_-\Big\}\Bigg], \tag{3.8a}$$

$$Y_{out} = \frac{\kappa_o + i\omega - 2G}{\kappa_o - i\omega + 2G}\Bigg[Y_{in} + M_3\Big\{\dot{\phi}_+ + \dot{\phi}_-\Big\}\Bigg], \tag{3.8b}$$

where $\dot{\phi}_{\pm} = \dot{\phi}(\pm\omega)$ while the parameters U, K, F_{SQL}, M_1, M_2 and M_3 are the same as given in Appendix A.

The first term in Eq. (3.8a) is the photons shot noise, while the second term is the radiation back action term, the third term is the external force signal normalized to F_{SQL} and the last two terms arise due to the PA's pump phase noise. Equation (3.8b) shows that the phase quadrature of the output field also contains the phase noise terms in addition to the back-action term. It may be noted that in the absence of PA (i.e., $G = 0$), Eqs. (3.8a), (3.8b) reduce to the same results as discussed in Ref. [43]. We can also define a generalized quadrature of the output field as $Z_{out}(\omega) = X_{out}(\omega)\cos\varphi + Y_{out}(\omega)\sin\varphi$, where φ represents the homodyne phase angle determined by the local oscillator that can be optimized for better sensitivity. By using Eq. (3.8a) and Eq. (3.8b), we obtained the following expression for the generalized quadrature:

$$\begin{aligned} Z_{out}(\omega) &= \frac{\kappa_o + i\omega + 2G}{\kappa_o - i\omega - 2G}\Bigg[X_{in}\cos\varphi + \Big(K\cos\varphi + \frac{1}{A}\sin\varphi\Big)Y_{in} \\ &+ \sqrt{2K}U\frac{f_{ex}}{F_{SQL}}\cos\varphi - M_1\cos\varphi \times (\dot{\phi}_+ - \dot{\phi}_-) \\ &+ \Big(-M_2\cos\varphi + \frac{M_3}{A}\sin\varphi\Big)(\dot{\phi}_+ + \dot{\phi}_-)\Bigg], \end{aligned} \tag{3.9}$$

where $A = \frac{(\kappa_o+2G)^2+\omega^2}{(\kappa_o-2G)^2+\omega^2}$. It is clear from Eq. (3.9) that it contains information about the weak force signal that can be detected by using homodyne detection of the quadrature $Z_{out}(\omega)$ of the output field from the cavity. Using the correlation

functions of the input vacuum noise

$$\langle X_{in}(\omega)X_{in}(\Omega)\rangle = \langle Y_{in}(\omega)Y_{in}(\Omega)\rangle = \frac{1}{2}2\pi\delta(\omega+\Omega), \tag{3.10a}$$

$$\langle X_{in}(\omega)Y_{in}(\Omega)\rangle = \langle Y_{in}(\omega)X_{in}(\Omega)\rangle = \frac{i}{2}2\pi\delta(\omega+\Omega), \tag{3.10b}$$

the spectrum of the fluctuations in the quadrature $Z_{out}(\omega)$ of the output field can be written as [43]

$$2\pi S_{out}(\omega)\delta(\omega+\Omega) = \frac{1}{2}\big[\langle Z_{out}(\omega)Z_{out}(\Omega)\rangle \quad + \quad \langle Z_{out}(\Omega)Z_{out}(\omega)\rangle\big]. \tag{3.11}$$

Finally, we obtain the following expression for the spectrum of the output field:

$$S_{out}(\omega) = 2AK\cos^2\varphi\left[\frac{1}{4K} + \frac{1}{4K}\left\{K + \frac{\tan\varphi}{A}\right\}^2 + \frac{1}{2K}S_{ph}(\omega) + f_s\right], \tag{3.12}$$

where $f_s = \frac{S_{ex}(\omega)}{F^2_{SQL}}$ is the spectrum of the external signal force normalized by the spectral density of SQL of force. When $f_s = 1$, the signal is said to be at SQL. $S_{ph}(\omega)$ is the noise spectrum of PA's drive and is given by

$$\begin{aligned} S_{ph}(\omega) \quad &= \quad \frac{2\Gamma_l}{1+\frac{\omega^2}{\gamma_c^2}}\left[\left\{-M_1 - M_2 + \frac{M_3\tan\varphi}{A}\right\}\left\{M_1' - M_2' + \frac{M_3'\tan\varphi}{A}\right\}\right. \\ &+ \quad \left.\left\{M_1 - M_2 + \frac{M_3\tan\varphi}{A}\right\}\left\{-M_1' - M_2' + \frac{M_3'\tan\varphi}{A}\right\}\right] \end{aligned} \tag{3.13}$$

where M_1', M_2' and M_3' are defined as

$$\begin{aligned} M_1' &= \frac{2c_sG\sqrt{\kappa_o}}{-\omega(\kappa_o - i\omega + 2G)}, \\ M_2' &= \frac{iGKc_s(\kappa_o - 2G)}{-\sqrt{\kappa_o}\omega(4G + i\omega)}, \\ M_3' &= \frac{2ic_sG\sqrt{\kappa_o}}{-\omega(\kappa_o - i\omega - 2G)}. \end{aligned} \tag{3.14}$$

In Eq. (3.12), the first term is the photon shot noise, the second term is the radiation back action noise, the third term is the noise associated with the phase fluctuation of PA's pump and the last term is the force signal. For the detection of force signal, the Fourier component of the noise should be smaller than the SQL normalized signal term. Hence the first three terms in Eq. (3.12) represent the

single sided spectral density of the noise i.e.,

$$S_N(\omega) = \frac{1}{4K}\Big[1 + \Big\{K + \frac{\tan\varphi}{A}\Big\}^2\Big] + \frac{1}{2K}S_{ph}(\omega), \tag{3.15}$$

by this definition when $S_N(\omega) = f_s = 1$, the noise level is said to be at SQL. Moreover, the homodyne phase angle φ can also be optimized at some frequency ω_o, to get rid of the back action term [93, 94, 96, 97]. The optimum homodyne angle φ_{opt} is given by

$$\tan\varphi_{opt} = -AK = \frac{J\kappa_o^2(16G^2 + \omega_o^2)}{\omega_o^2[(\kappa_o - 2G)^2 + \omega_o^2]}. \tag{3.16}$$

where $J = \frac{\hbar\eta^2 c_s^2}{m\kappa_o}$ is dimensionless power parameter and is proportional to the input power (See Appendix A). Thus, on substituting Eq. (3.16) into Eq. (3.15), the back action term can be completely eliminated at $\omega = \omega_o$. It may also be noted that when phase noise is zero, our result reduces to that of Huang et al. [43]. If we further simplify our system by assuming that the gain of PA is also zero i.e., $G = 0$, our results reduces to that of Vyatchanin et al. [42].

3.3 Results and Discussion

Next, we present the results of our numerical simiulation. Throughout in our calculations, we consider $m = 100$ ng, $\kappa_o = 2\pi$ MHz, $\lambda = 1064$ nm and $\eta = 4.182 \times 10^8$ m^{-1} which are the same as discussed in Ref. [43]. In our analysis, we also keep the system in the stable regime i.e., $G/\kappa_o < 1/2$. The power parameter J can be written as $J = J_o(1 - 2G/\kappa_o)^{-2}$, where J_o refers to the power parameter in the absence of PA (See Appendix A). In Fig. (3.1), the dotted line shows the noise spectrum S_N when gain of PA is zero i.e. $G = 0$, the noise spectrum S_N is below the SQL line and is approximately -3 dB around the homodyne phase φ_{opt} is optimized at $\omega/\kappa_o = 1$. This is the case which has been discussed in detail in Ref [42]. When gain of the parametric amplifier is non-zero i.e., $G/\kappa_o = 0.2$ (dashed line), the noise spectrum drops to -9 dB around the homodyne phase. Thus, the presence of PA greatly improves the force sensitivity as discussed in detail in Ref. [43]. Next we consider the effect of phase fluctuations associated with

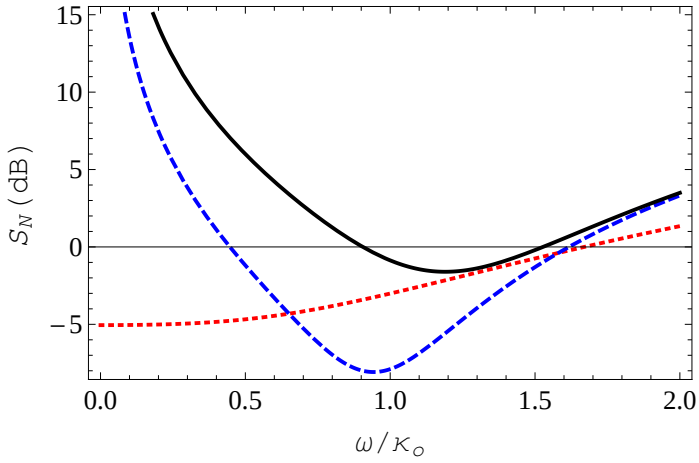

Figure 3.1: Here the dotted line shows noise spectrum in the absence of PA, the dashed line corresponds to the noise spectrum when PA is used for the force detection and the solid line represents the noise spectrum in presence of phase fluctuations associated with the pump driving the PA. The horizontal line corresponds to SQL. Here $J_o = 1$, $G/\kappa_o = 0.2$, $\Gamma_l = 100$ Hz, $\gamma_c = 500$ Hz and the homodyne angle is set at $\omega/\kappa_o = 1$.

the pump laser which drives PA. The solid line in Fig. (3.1) corresponds to the case when pump phase fluctuation is non-zero i.e., $\Gamma_l = 100$ Hz and $\gamma_c = 500$ Hz. The result clearly shows that S_N is still below SQL line however, with less sensitivity and smaller bandwidth. It is clear that the phase noise associated with PA pump considerably reduces the sensitivity for below SQL measurement. Here the power parameter $J_o = 1$ and the homodyne phase defined by Eq. (3.16), is optimized at $\omega/\kappa_o = 1$ in all the three cases.

To further elaborate the effects of PA's pump phase noise, consider Fig. (3.2) which shows a contour plot of the noise spectrum S_N against the laser linewidth Γ_l and the noise correlation parameter γ_c. The contour at $S_N = 0$ (as shown by white line) is at SQL while the region below this contour (dark shaded region) corresponds to below SQL regime. In order to achieve sensitivity below SQL, the values of Γ_l and γ_c should be selected in the dark shaded region.

Next, Fig. (3.3) shows contour plots of the noise spectrum S_N against the parametric gain G/κ_o and the detection frequency ω/κ_o. The solid line refers to the case when phase fluctuation is zero and the sensitivity is at SQL. By increasing the parametric gain such that $0 \leq G/\kappa_o < 0.5$, the range of detection frequency

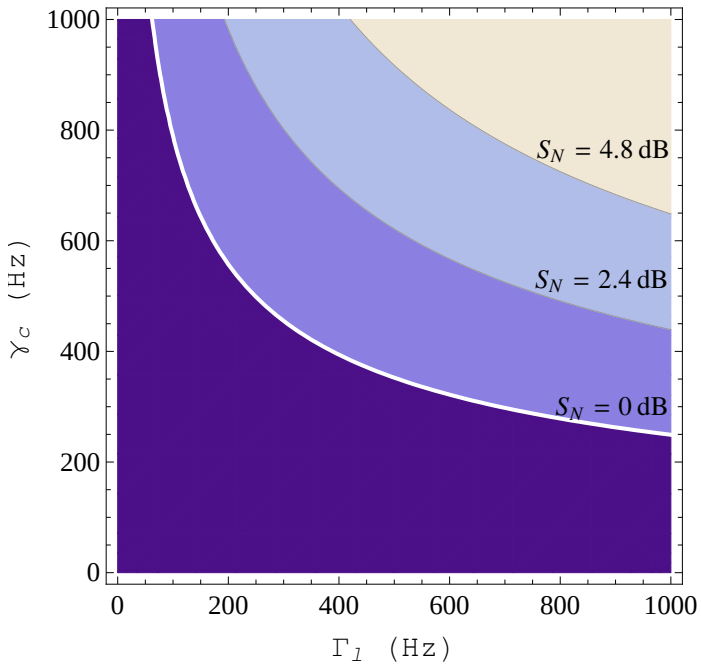

Figure 3.2: Contour plot of the noise spectrum S_N against laser linewidth Γ_l and noise correlation parameter γ_c. Here $S_N = 0$ dB (contour shown by white line) corresponds to SQL and the region below this contour (the darkest one) gives better than SQL sensitivity. Here $J_o = 0.25$ and other parameters are the same as in Fig. (3.1).

increases and then start decreasing and eventually approaches to the limiting value of $\omega/\kappa_o \approx 1$. The detection frequency range is maximum when parametric gain is around $0.15 < G/\kappa_o < 0.3$. We can have below SQL sensitivity for almost any value of the parametric gain (between $0 < G/\kappa_o < 0.5$) and for each value of the parametric gain we have certain width of detection frequency range. However, our results show that when phase noise is also incorporated, the range of detection frequency and parametric gain for which SQL can be beaten is reduced. This is shown by dot-dashed, dashed and dotted contours in Fig. (3.3). Depending upon the values of Γ_l and γ_c, we have different size of contours and therefore, limited freedom in selecting various parameters for achieving below SQL sensitivity. Thus measurement sensitivity is determined by the laser linewidth and noise correlation parameter.

Figure (3.4) shows contour plots of the noise spectrum S_N against the parametric gain G/κ_o and the power parameter J_o. The homodyne phase is optimized at $\omega/\kappa_o = 1$. The solid line corresponds to the case when pump phase noise is

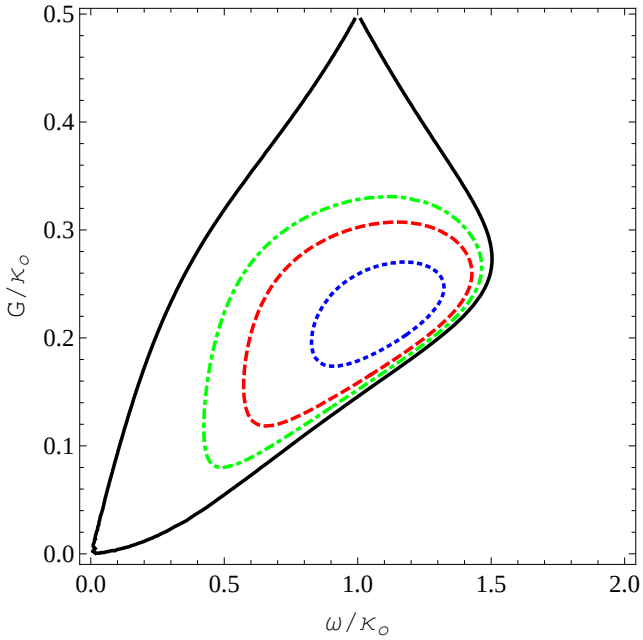

Figure 3.3: Contour plots of noise spectrum S_N against parametric gain G/κ_o and detection frequency ω/κ_o. Here all the contours are at SQL. The solid contour corresponds to the case when phase fluctuation of the PA's pump is zero. The dotted, dashed and dot-dashed contours correspond to ($\Gamma_l = 50$ Hz, $\gamma_c = 1000$ Hz), ($\Gamma_l = 100$ Hz, $\gamma_c = 500$ Hz) and ($\Gamma_l = 150$ Hz, $\gamma_c = 300$ Hz), respectively. Here $J_o = 0.25$ and all the other parameters are the same as in Fig. (3.1).

zero. By increasing the parametric gain the minimum power required to achieve SQL decreases. However, when phase fluctuation of the PA's pump is not zero, we have both upper and lower bound on the power parameter for below SQL measurement. For instance, when $\Gamma_l = 100$ Hz and $\gamma_c = 500$ Hz (dashed contour), then for $G/\kappa_o = 0.2$ the power range allowed for below SQL sensitivity is $0.18 < J_o < 1.18$. And for $\Gamma_l = 50$ Hz and $\gamma_c = 1000$ Hz (dotted contour) at $G/\kappa_o = 0.2$ the allowed power range for below SQL sensitivity is $0.21 < J_o < 0.71$. Similarly, for $\Gamma_l = 150$ Hz and $\gamma_c = 300$ Hz (dot-dashed contour) at $G/\kappa_o = 0.2$, below SQL sensitivity can be achieved for $0.17 < J_o < 1.7$. Thus the presence of phase noise not only limits the parametric gain but also affects the power range for below SQL sensitivity.

Figure (3.5) shows contour plots of the noise spectrum S_N against the power parameter J_o and the detection frequency ω/κ_o. The parametric gain is $G/\kappa_o = 0.2$. The solid line corresponds to the case when pump phase noise is zero. By

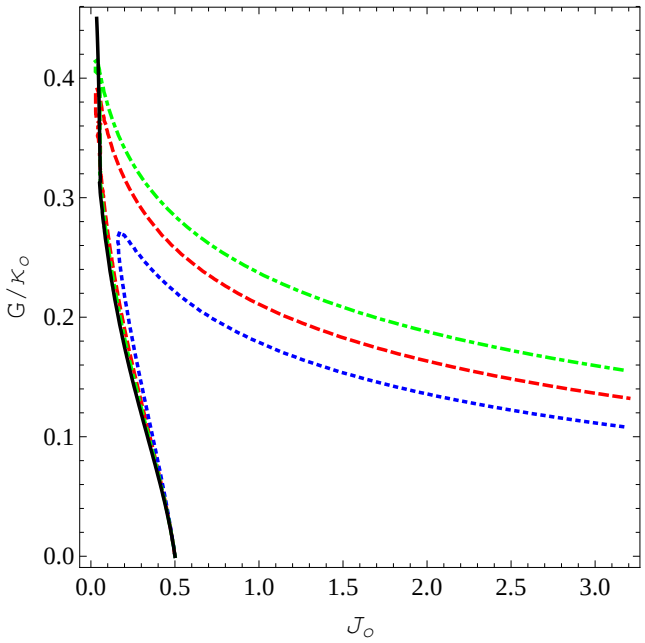

Figure 3.4: Contour plots of noise spectrum S_N against the parametric gain G/κ_o and power parameter J_o. Here all the contours are at SQL. The solid contour corresponds to the case when phase fluctuation of the PA's pump is zero. The dotted, dashed and dot-dashed contours correspond to ($\Gamma_l = 50$ Hz, $\gamma_c = 1000$ Hz), ($\Gamma_l = 100$ Hz, $\gamma_c = 500$ Hz) and ($\Gamma_l = 150$ Hz, $\gamma_c = 300$ Hz), respectively. Here the homodyne phase is optimized at $\omega/\kappa_o = 1$ and all the other parameters are the same as in Fig. (3.1).

increasing the input power the detection frequency range decreases but in a very slow fashion for instance, at power level of $J_o = 3$, the detection frequency is in the range of $0.6 < \omega/\kappa_o < 1.4$. It is also interesting to note that for $J_o = 0.25$, the detection frequency range is $0.25 < \omega/\kappa_o < 1.32$ (which can also be verified from Fig. (3.3) at $G/\kappa_o = 0.2$). However, when phase fluctuation of the PA's pump is not zero, not only the detection frequency range is reduced but the range of power level is also reduced for below SQL measurement. For instance, when $\Gamma_l = 100$ Hz and $\gamma_c = 500$ Hz (dashed contour), then for $G/\kappa_o = 0.2$ the power range allowed for below SQL sensitivity is $0.18 < J_o < 1.18$ at detection frequency of $\omega/\kappa_o = 1$. Furthermore, for $\Gamma_l = 50$ Hz and $\gamma_c = 1000$ Hz (dotted contour), the allowed power range for below SQL sensitivity is $0.21 < J_o < 0.71$ at $G/\kappa_o = 0.2$ and $\omega/\kappa_o = 1$. Similarly, for $\Gamma_l = 150$ Hz and $\gamma_c = 300$ Hz (dot-dashed contour), below SQL sensitivity can be achieved for $0.17 < J_o < 1.7$. All these results are consistent with Fig. (3.4). The power range for below SQL sensitivity is maximum

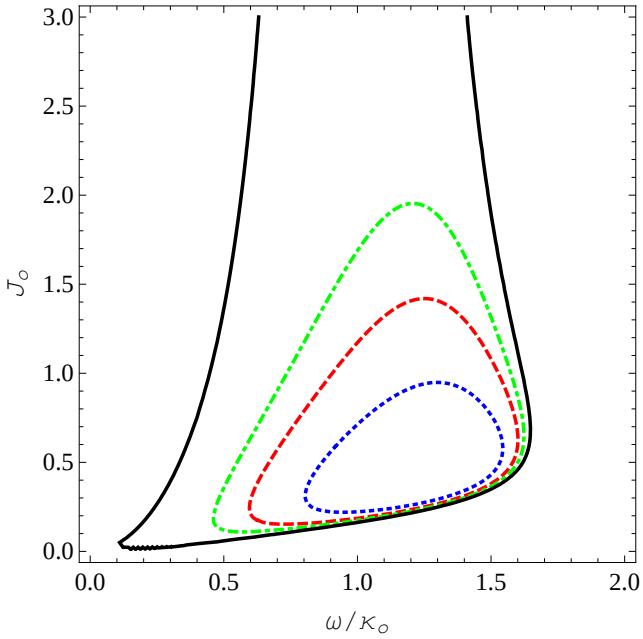

Figure 3.5: Contour plots of noise spectrum S_N against power parameter J_o and detection frequency ω/κ_o. All the contours are at SQL. The solid contour corresponds to the case when phase fluctuation of the PA's pump is zero. The dotted, dashed and dot-dashed contours correspond to (Γ_l = 50 Hz, γ_c = 1000 Hz), (Γ_l = 100 Hz, γ_c = 500 Hz) and (Γ_l = 150 Hz, γ_c = 300 Hz) respectively. Here $G/\kappa_o = 0.2$ and all other parameters are the same as in Fig. (3.1).

for the detection frequency in the neighborhood of optimum phase as back-action is minimum around that phase.

Figure (3.6) shows the plot of noise spectrum against the detection frequency for different choices of various parameters. The dot-dashed curve shows the noise spectrum when Γ_l = 500 Hz, γ_c = 1 KHz, J_o = 1 and the optimum angle is set at ω/κ_o = 2. For dashed curve, Γ_l = 1 KHz, γ_c = 5 KHz, J_o = 10 and the optimum angle is set at ω/κ_o = 7. For solid curve, Γ_l = 2 KHz, γ_c = 10 KHz, J_o = 15 and the optimum angle is ω/κ_o = 9. The parametric gain in all the three cases is $G/\kappa_o = 0.2$. It may be noted that by increasing the laser linewidth and noise correlation parameter, below SQL measurement is possible, however, it require higher values of input power and the optimum angle is shifted towards higher values of the detection frequency. It follows from above discussion that depending upon the values of Γ_l and γ_c, below SQL sensitivity can be achieved for specific range of input power J_o, detection frequency ω/κ_o and parametric gain

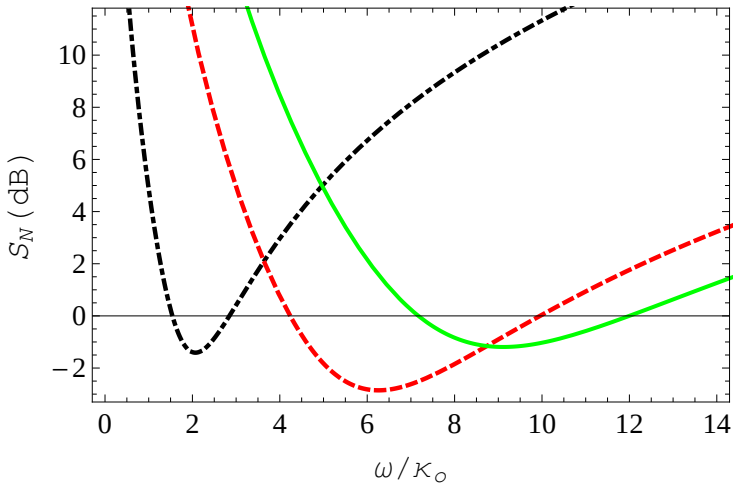

Figure 3.6: Plot of the noise spectrum S_N against the detection frequency ω/κ_o. For dot-dashed curve, $\Gamma_l = 500$ Hz, $\gamma_c = 1$ KHz, $J_o = 1$ and the optimum angle is set at $\omega/\kappa_o = 2$. For dashed curve, $\Gamma_l = 1$ KHz, $\gamma_c = 5$ KHz, $J_o = 10$ and the optimum angle is set at $\omega/\kappa_o = 7$. For solid curve, $\Gamma_l = 2$ KHz, $\gamma_c = 10$ KHz, $J_o = 15$ and the optimum angle is set at $\omega/\kappa_o = 9$. The parametric gain in all the three cases is $G/\kappa_o = 0.2$.

G/κ_o. Thus, the presence of LPN (associated with the PA pump) limits the choice of selection of various parameters for below SQL measurement.

3.4 Summary

To summarize the results in this chapter, we have considered the effect of phase fluctuations associated with the laser driving PA in a dissipatively coupled optomechanical system on force sensing. Our results show that the sensitivity of the force detection strongly depends upon the laser phase fluctuation associated with PA's pump. However, force measurement better than SQL can still be achieved with a wider frequency range provided an optimum choice of various parameters is made. As an example, for any particular value of the gain within $0 < G < 0.5$, there exists a certain range of the laser linewidth Γ_l and noise correlation parameter γ_c in which below SQL measurement is possible. And for below SQL sensitivity at that particular value of G, Γ_l and γ_c, there exist a certain range of input power level and detection frequency. Thus in case of LPN of PA pump, we have limited choice in the selection of various parameters for below SQL measurement.

Chapter 4

Effects of Kerr Medium on Force Sensing in a Dissipative Optomechanical System

4.1 Introduction

In this chapter, we study the effects of the Kerr medium on the detection of a weak classical force acting on an OM oscillator which is coupled purely dissipatively. The presence of Kerr medium inside an OM cavity can lead to very interesting effects such as controlling the normal mode splitting (NMS) due to photon blockade [80], enhancement of OM entanglement [81] and bistability of the OM system [82, 83]. In an earlier study, it has been shown that the use of Kerr cell in interferometric gravity-wave detector counters the radiation pressure induced fluctuations. The performance of such interferometers greatly surpass SQL [51]. We are therefore interested to see the effects of optical Kerr medium on force sensing in a dissipative OM system.

4.2 Theory and Model

We consider an optomechanical (OM) system where the oscillator of mass m and frequency ω_m is dissipatively coupled to a cavity field having eigenfrequency ω_o. The cavity is driven by a strong coherent light of frequency ω_l and amplitude ε_l. We assume an optical Kerr medium is present inside the OM cavity with anhormonicity parameter χ. For the realization of dissipative coupling, we consider the Michelson-Sagnac Interferometer (MSI) configuration as shown in Fig. (1.2) in Chapter 1. An interesting feature of this system is that it can be tuned to operate in pure dissipative coupling regime. This can be done by properly adjusting the

position of the membrane and the reflectivity of the beam splitter as discussed in detail by Xuereb et al. [54]. The Hamiltonian of the system in rotating frame at frequency ω_l is given by

$$\begin{aligned}\hat{H} &= \hbar\Delta_o c^\dagger c + \frac{1}{2}m\omega_m^2 x^2 + \frac{p^2}{2m} \\ &+ i\hbar\sqrt{2\kappa}[\varepsilon_l(c^\dagger - c) + c^\dagger c_{in} - c_{in}^\dagger c] + \hbar\chi c^{\dagger 2}c^2, \end{aligned} \tag{4.1}$$

where $\Delta_o = \omega_o - \omega_l$ and $\kappa = \kappa_o(1+\eta x)$, represents the position dependent photon decay rate and $\kappa = \kappa_o$ when $x = 0$. The parameter η is related to the dissipative coupling strength as $g_\kappa = \eta\kappa_o x_{zpf}$, where $x_{zpf} = \sqrt{\hbar/2m\omega_m}$ is the zero-point fluctuation of the oscillator. The amplitude of the field is related to the input power as $\varepsilon_l = \sqrt{\mathbb{P}/\hbar\omega_l}$. The first term in the Hamiltonian represents the free energy of the cavity field, while the second and third term represent the energy of the oscillator. The fourth term represents the coupling of cavity field with the input laser while the input vacuum noise is represented by c_{in}. The last term represents the interaction between the cavity field and the Kerr medium with $\chi \equiv 3\hbar\omega_o^2 Re[\chi^{(3)}]/2\epsilon V_c$, where ϵ represents the dielectric constant of the medium, V_c is the volume of the cavity and $\chi^{(3)}$ is the third order nonlinear susceptibility of the medium.

In the presence of an external weak force F_{ex} with zero mean value acting on the oscillator, the Heisenberg equations of motion for the system are given by the following:

$$\dot{x} = \frac{p}{m}, \tag{4.2a}$$

$$\dot{p} = -\frac{i\hbar\eta\sqrt{2\kappa_o}}{2}[\varepsilon_l(c^\dagger - c) + c^\dagger c_{in} - c_{in}^\dagger c] - m\omega_m^2 x - \gamma_m p + \xi + F_{ex}, \tag{4.2b}$$

$$\dot{c} = -i\Delta_o c + \sqrt{2\kappa_o}(1 + \frac{\eta}{2}x)(\varepsilon_l + c_{in}) - 2i\chi c^\dagger c^2 - \kappa_o(1+\eta x)c. \tag{4.2c}$$

In the steady-state, the solution of Eqs. (4.2a)-(4.2c) yields

$$p_s = 0,\ c_s = \frac{\sqrt{2\kappa_s}\varepsilon_l}{\kappa_s + i\Delta},\ x_s = \frac{\sqrt{2\kappa_o}i\hbar\eta\varepsilon_l(c_s - c_s^*)}{2m\omega_m^2}, \tag{4.3}$$

where $\kappa_s = \kappa_o(1+\eta x_s)$, $\Delta = \Delta_o + 2\chi N_s$ and $N_s = |c_s|^2$. It may be noted that both x_s and N_s are not only related to each other but also satisfies third order

equation and can have three roots, as a result, it can display multistable behavior. The steady-state photon density N_s must be real and positive, while the steady state position x_s of the oscillator must be real. It is also clear from Eq. (4.3), when $\Delta = 0 \Rightarrow c_s = c_s^*$ which leads to $x_s = 0$. The operators given by Eqs. (4.2a)-(4.2c) can be represented as a sum of large mean value and small fluctuating terms such that $x = x_s + \delta x = \delta x$, $p = p_s + \delta p = \delta p$ and $c = c_s + \delta c$. In the first order approximation, the linearized equations of motion are given by the following:

$$\delta\dot{x} = \frac{\delta p}{m}, \tag{4.4a}$$

$$\delta\dot{p} = -\frac{i\hbar\eta\sqrt{2\kappa_o}}{2}[\varepsilon_l(\delta c^\dagger - \delta c) + c_s^* c_{in} - c_s c_{in}^\dagger)] - m\omega_m^2\delta x - \gamma_m\delta p + \xi + F_{ex}, \tag{4.4b}$$

$$\delta\dot{c} = -[\kappa_s + i(\Delta_o + 4\chi N_s)]\delta c - 2i\chi c_s^2\delta c^\dagger + \frac{(\kappa_o\eta x_s/2 + i\Delta)c_s\eta\delta x}{1 + \eta x_s/2} + \sqrt{2\kappa_s}c_{in}. \tag{4.4c}$$

Equations (4.4a)-(4.4c) and their Hermitian conjugate constitute a system of four first order coupled equations which can be written as

$$\dot{f}(t) = Af(t) + \zeta(t), \tag{4.5}$$

where $f(t)$ and $\zeta(t)$ are column vectors and their transposes are given by

$$\begin{aligned} f(t)^T &= (\delta x,\ \delta p,\ \delta c,\ \delta c^\dagger), \\ \zeta(t)^T &= (0,\ \frac{i\hbar\eta\sqrt{2\kappa_o}}{2}[c_s c_{in}^\dagger - c_s^* c_{in}] + \xi + F_{ex},\ \sqrt{2\kappa_s}c_{in},\ \sqrt{2\kappa_s}c_{in}^\dagger), \end{aligned} \tag{4.6}$$

while matrix A is given by

$$A = \begin{bmatrix} 0 & 1/m & 0 & 0 \\ -m\omega_m^2 & -\gamma_m & iW & -iW \\ -c_1/\sqrt{2} & 0 & -\kappa_1 & -2i\chi c_s^2 \\ -c_1^*/\sqrt{2} & 0 & 2i\chi c_s^{*2} & -\kappa_1^* \end{bmatrix}, \tag{4.7}$$

where $c_1 = \sqrt{2}\eta c_s(\kappa_o\eta x_s/2 + i\Delta)/(1 + \eta x_s/2)$, $\kappa_1 = \kappa_s + i(\Delta + 2\chi N_s)$ and $W = \sqrt{2\kappa_o}\hbar\eta\varepsilon_l/2$. The solution of Eq. (4.5) is $f(t) = M(t)f(0) + \int_0^{t'} M(t')\zeta(t - t')dt'$,

where $M(t) = e^{At}$. The system reaches its steady-state value and remains stable as $t \to \infty$ only if the real parts of all the eigenvalues of the matrix A are negative such that $M(\infty) = 0$. The stability conditions for the system can be obtained by employing the Routh-Hurwitz criterion [99], and are given by

$$\begin{aligned} S_1 &= 2\sqrt{2}m\kappa_s[(\kappa_s+\gamma_m)^2+\Delta(\Delta+4\chi N_s)]+\sqrt{2}m\gamma_m\omega_m^2 - iW(c_1-c_1^*) > 0, \\ S_2 &= iW(c_1\kappa_1^* - c_1^*\kappa_1) - 2W\chi(c_s^2c_1^* + c_s^{*2}c_1) + \sqrt{2}m\omega_m^2[\kappa_s^2+\Delta(\Delta+4\chi N_s)] > 0, \\ S_3 &= \left[iW(c_1-c_1^*)+\sqrt{2}m\gamma_m\left\{\kappa_s^2+\Delta(\Delta+4\chi N_s)\right\}+2\sqrt{2}\kappa_s m\omega_m^2\right]S_1 \\ &- \sqrt{2}m^2(2\kappa_s+\gamma_m)^2S_2 > 0. \end{aligned} \tag{4.8}$$

Throughout our numerical analysis we restrict to the stable regime. All the parameters chosen in this work have been verified to satisfy the stability conditions given by Eq. (4.8).

Next we take the Fourier transform of the operators given by Eqs. (4.4a)-(4.4c). As a result, fluctuations in the position of oscillator and cavity field in frequency domain are found to be

$$\begin{aligned} \delta x(\omega) = Z(\omega)\Bigg[&- \frac{iW}{\varepsilon_l}\left\{\varepsilon_l(\delta c^\dagger(\omega)-\delta c(\omega)) + c_s^* c_{in}(\omega) - c_s c_{in}^\dagger(\omega)\right\} \\ &+ \xi(\omega) + f_{ex}(\omega)\Bigg], \end{aligned} \tag{4.9a}$$

$$\delta c(\omega) = \frac{\sqrt{2\kappa_s}c_{in}(\omega) - 2i\chi c_s^2\delta c^\dagger(-\omega) + c_1\delta x(\omega)/\sqrt{2}}{(\kappa_1 - i\omega)}, \tag{4.9b}$$

where $Z^{-1}(\omega) = m(\omega_m^2 - \omega^2 - i\omega\gamma_m)$ is the susceptibility of the mechanical oscillator. Defining the input amplitude and phase quadratures as $X_{in}(\omega) = \frac{1}{\sqrt{2}}[c_{in}(\omega) + c_{in}^\dagger(-\omega)]$ and $Y_{in}(\omega) = \frac{1}{i\sqrt{2}}[c_{in}(\omega) - c_{in}^\dagger(-\omega)]$. Similarly, for the field inside the cavity, the amplitude and phase quadratures are defined as $X(\omega) = \frac{1}{\sqrt{2}}[\delta c(\omega) + \delta c^\dagger(-\omega)]$ and $Y(\omega) = \frac{1}{i\sqrt{2}}[\delta c(\omega) - \delta c^\dagger(-\omega)]$. By using these definitions, Eq. (4.9b) can be written in terms of quadratures of the field as follows

$$a_1(\omega)X(\omega) + ib_1(\omega)Y(\omega) = c_1(\omega)\delta x + \sqrt{2\kappa_s}\{X_{in}(\omega) + iY_{in}(\omega)\}, \tag{4.10}$$

where $a_1(\omega) = \kappa_1 + i(2\chi c_s^2 - \omega)$ and $b_1(\omega) = a_1(\omega) - 4i\chi c_s^2$. By solving Eq. (4.10) along with its Hermitian conjugate, we obtain the following expressions for the

quadratures of the cavity field:

$$X(\omega) = \frac{1}{a_2(\omega)}\Big[a_3(\omega)\delta x(\omega) + \sqrt{2\kappa_s}\Big(\{b_1(\omega) + b_1^*(-\omega)\}X_{in}(\omega) - i\{b_1(\omega) - b_1^*(-\omega)\}Y_{in}(\omega)\Big)\Big], \tag{4.11a}$$

$$Y(\omega) = \frac{i}{a_2(\omega)}\Big[a_4(\omega)\delta x(\omega) + \sqrt{2\kappa_s}\Big(\{a_1(\omega) - a_1^*(-\omega)\}X_{in}(\omega) - i\{a_1(\omega) + a_1^*(-\omega)\}Y_{in}(\omega)\Big)\Big], \tag{4.11b}$$

where

$$\begin{aligned} a_2(\omega) &= a_1(\omega)b_1^*(-\omega) + a_1^*(-\omega)b_1(\omega), \\ a_3(\omega) &= b_1(\omega)c_1^* + b_1^*(-\omega)c_1, \\ a_4(\omega) &= a_1(\omega)c_1^* - a_1^*(-\omega)c_1. \end{aligned} \tag{4.12}$$

The position fluctuation can also be written in terms of input amplitude and phase quadrature as

$$\delta x(\omega) = Z_{eff}(\omega)\Big[-a_5(\omega)X_{in} + a_6(\omega)Y_{in} + \xi(\omega) + f_{ex}(\omega)\Big], \tag{4.13}$$

where $a_5(\omega)$ and $a_6(\omega)$ are as follows,

$$\begin{aligned} a_5(\omega) &= i\hbar\eta\sqrt{\kappa_o}\Big[\frac{c_s - c_s^*}{2} + \frac{\varepsilon_l\sqrt{2\kappa_s}(a_1(\omega) - a_1^*(-\omega))}{a_2(\omega)}\Big], \\ a_6(\omega) &= \hbar\eta\sqrt{\kappa_o}\Big[\frac{c_s + c_s^*}{2} - \frac{\varepsilon_l\sqrt{2\kappa_s}(a_1(\omega) + a_1^*(-\omega))}{a_2(\omega)}\Big], \end{aligned} \tag{4.14}$$

and $Z_{eff}^{-1}(\omega) = m(\Omega_{eff}^2 - \omega^2 - i\omega\Gamma_{eff})$ is the effective susceptibility of the oscillator in the presence of Kerr medium with effective mechanical frequency $\Omega_{eff}^2 = \omega_m^2 + Re[K(\omega)]$ and effective mechanical damping $\Gamma_{eff} = \gamma_m - Im[K(\omega)]/\omega$. Here the parameter $K(\omega)$ is defined as $K(\omega) = i\hbar\eta\varepsilon_l\sqrt{\kappa_o}a_4(\omega)/[ma_2(\omega)]$. It may be noted that $\Delta = 0$ leads to $K(\omega) = 0$ and eventually $Z_{eff}(\omega) = Z(\omega)$. In Eq. (4.13), the first two terms arise due to the input vacuum noise, the third term represents the contribution of the thermal noise and the last term is due to the external force. In the absence of dissipative coupling and external force, the oscillator follows

Brownian motion, and the spectral density is Lorentzian centered at frequency ω_m with full width of γ_m at half maximum.

Using Eq. (3.6b) for fluctuating output field and defining the fluctuating quadrature of the output field as $X_{out}(\omega) = [c_{out}(\omega) + c^{\dagger}_{out}(-\omega)]/\sqrt{2}$ and $Y_{out}(\omega) = [c_{out}(\omega) - c^{\dagger}_{out}(-\omega)]/i\sqrt{2}$, we obtain the following expressions for the amplitude and phase quadrature of the output field:

$$X_{out}(\omega) = \sqrt{2\kappa_o}X(\omega) + \frac{\sqrt{\kappa_o}\eta(c_s + c_s^*)}{2}\delta x(\omega) - X_{in}(\omega), \tag{4.15a}$$

$$Y_{out}(\omega) = \sqrt{2\kappa_o}Y(\omega) + \frac{\sqrt{\kappa_o}\eta(c_s - c_s^*)}{2i}\delta x(\omega) - Y_{in}(\omega). \tag{4.15b}$$

On substituting Eqs. (4.11a), (4.11b) and (4.13) into Eqs. (4.15a) and (4.15b), the output quadratures of the field are found to be

$$X_{out}(\omega) = h_1(\omega)X_{in}(\omega) + h_2(\omega)Y_{in}(\omega) + h_3(\omega)\left\{\xi(\omega) + f_{ex}(\omega)\right\}, \tag{4.16a}$$

$$Y_{out}(\omega) = h_4(\omega)X_{in}(\omega) + h_5(\omega)Y_{in}(\omega) + h_6(\omega)\left\{\xi(\omega) + f_{ex}(\omega)\right\}, \tag{4.16b}$$

where the parameters $h_1(\omega)$, $h_2(\omega)$, $h_3(\omega)$, $h_4(\omega)$, $h_5(\omega)$ and $h_6(\omega)$ in Eqs. (4.16a) and (4.16b) are defined in Appendix B.

It may be noted that in the absence of Kerr medium the shot noise and thermal noise are present only in the amplitude quadrature of the output field as can be seen in Ref. [42, 43]. However, Eqs. (4.16a) and (4.16b) show that in the presence of Kerr medium, both quadratures contain the shot noise, back action, thermal noise and external force signal. This interesting feature arises due to the fact that the optical Kerr medium transforms amplitude fluctuations in the initial coherent state into phase fluctuations [90]. We can also define a generalized quadrature of the output field as $Z_{out}(\omega) = X_{out}(\omega)\cos\varphi + Y_{out}(\omega)\sin\varphi$, where φ represents the homodyne phase angle determined by the local oscillator that can be optimized for better sensitivity. By using Eqs. (4.16a) and (4.16b), we obtained the following

expression for the generalized quadrature:

$$\begin{aligned} Z_{out}(\omega) &= \big[h_1(\omega)\cos\varphi + h_4(\omega)\sin\varphi\big]X_{in}(\omega) \\ &+ \big[h_2(\omega)\cos\varphi + h_5(\omega)\sin\varphi\big]Y_{in}(\omega) \\ &+ \big[h_3(\omega)\cos\varphi + h_6(\omega)\sin\varphi\big][\xi(\omega) + f_{ex}(\omega)]. \end{aligned} \tag{4.17}$$

Equation (4.17) shows that the generalized quadrature contains information about the weak force signal. It can be detected by using homodyne detection of the quadrature $Z_{out}(\omega)$ of the output field from the cavity. In order to elliminate the back-action noise [93, 94, 97], the homodyne phase φ can be optimized by setting $\tan\varphi_{opt} = -h_2(\omega)/h_5(\omega)$. We assume the input light is in a coherent state and MSI operates in its dark port condition. Under this assumption $S_{X_{in}} = S_{Y_{in}} = 1$ and there is no correlation between X_{in} and Y_{in} [40, 54]. Using these correlations and Eq. (3.11) in Chapter 3, the spectral density of the fluctuation in the quadrature $Z_{out}(\omega)$ of the output field can be written as

$$S_{out}(\omega) = \frac{1}{2}\big[S_{sh}(\omega) + S_{ba}(\omega) + S_{th}(\omega) + S_{ex}(\omega)\big], \tag{4.18}$$

where S_{sh}, S_{ba}, S_{th} and S_{ex} represent the spectral density of shot noise, back action, thermal noise and external signal force respectively. The thermal noise contribution is given by $S_{th} = \langle\xi(\omega)\xi(\omega')\rangle = 4\pi m K_B T\gamma_m\delta(\omega+\omega')$ while S_{sh} and S_{ba} are given by

$$\begin{aligned} S_{sh}(\omega) &= \left|\frac{h_1(\omega)\cos\varphi + h_4(\omega)\sin\varphi}{h_3(\omega)\cos\varphi + h_6(\omega)\sin\varphi}\right|^2, \\ S_{ba}(\omega) &= \left|\frac{h_2(\omega)\cos\varphi + h_5(\omega)\sin\varphi}{h_3(\omega)\cos\varphi + h_6(\omega)\sin\varphi}\right|^2. \end{aligned} \tag{4.19}$$

In order to detect the force signal below SQL, the Fourier component of the noise should be smaller than SQL normalized signal term i.e. $S_{sh} + S_{ba} + S_{th} \leq S_{ex}/S_{sql}$. Thus the noise term can be written as

$$S_N(\omega) = \frac{1}{S_{sql}}(S_{sh} + S_{ba} + S_{th}), \tag{4.20}$$

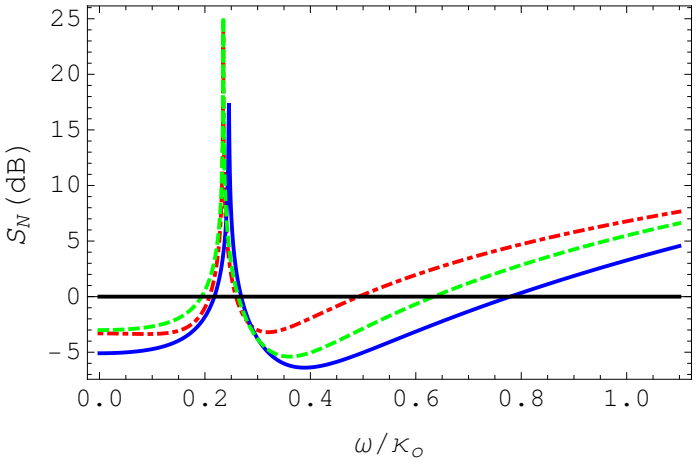

Figure 4.1: Noise spectrum S_N against detection frequency ω/κ_o. Here, red (dot-dashed), green (dashed) and blue (solid) line shows noise spectrum for $\Delta_o = \chi N_s = 0$, $\Delta_o = -2\chi N_s = -0.3\kappa_o$ and "$\chi N_s/\kappa_o = 0.15$, $\Delta_o = 0$", respectively. The solid straight line corresponds to the oscillator's SQL of force. Here we used $P = 1$ watt and $T = 0.1$ K.

where $S_{sql} = 2m\hbar\sqrt{(\Omega_{eff}^2 - \omega^2)^2 + \Gamma_{eff}^2\omega^2}$ (in units of N^2/Hz) is the SQL of force for the mechanical oscillator. In the special case, when $\Delta = 0$, we have $S_{sql} = 2m\hbar\sqrt{(\omega_m^2 - \omega^2)^2 + \gamma_m^2\omega^2}$. The noise level is said to be at SQL when $S_N = 1$.

4.3 Results and Discussion

Next, we present the results of our numerical simiulation. We use the parameters $m = 100$ ng, $\kappa_o = 2\pi$ MHz, $\omega_m/\kappa_o = 0.2348$, $\lambda = 1064$ nm, $\eta = 4.182 \times 10^8$ m^{-1} and $\gamma_m/\kappa_o = 10^{-5}$ as discussed in Ref. [43]. In Fig. (4.1), we have plotted the noise spectrum S_N of the output field against the detection frequency ω/κ_o for three different cases: (i) when the cavity is driven resonantly in the absence of Kerr medium i.e., $\Delta_o = \chi N_s = 0$ (dot-dashed curve), (ii) when the cavity is driven resonantly in the presence of Kerr medium i.e., $\Delta_o = 0$, $\chi N_s/\kappa_o = 0.15$ (solid curve) and (iii) when the cavity is detuned in the presence of Kerr medium such that $\Delta_o = -2\chi N_s = -0.3\kappa_o$ (dashed curve). Clearly, when the cavity is driven resonantly in the presence of Kerr medium, it not only improves the force sensitivity but also the detection frequency range as compared to the case when Kerr medium is not present (please see solid and dot-dashed curves). The presence of Kerr medium makes the system more sensitive to the power P, detuning Δ_o and

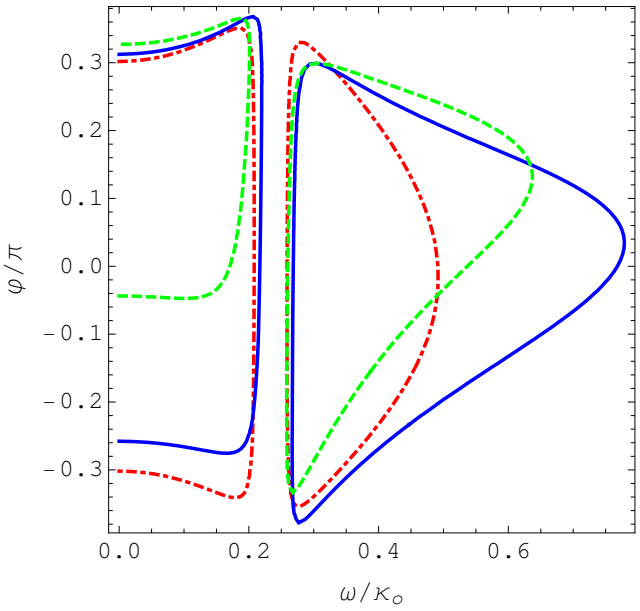

Figure 4.2: Contour plot of noise spectrum S_N against detection frequency ω/κ_o and detection phase φ/π. Here, red (dot-dashed), green (dashed) and blue (solid) contour correspond to $\Delta_o = \chi N_s = 0$, $\Delta_o = -2\chi N_s = -0.3\kappa_o$ and "$\chi N_s/\kappa_o = 0.15$, $\Delta_o = 0$", respectively. All the contours are at SQL i.e., $S_N = 0$ dB. All the other parameters are the same as in Fig. (4.1).

the strength of Kerr non-linearity χN_s. The stability condition given by Eq. (4.8) must be fulfilled for various choices of parameters to keep the system stable. As we discussed earlier, Eq. (4.3) shows that when $\Delta = \Delta_o + 2\chi N_s \neq 0$, the steady-state amplitude of the cavity field c_s and the steady state position of the oscillator x_s are related to each other and can show multistable behavior for some values of various parameters. An interesting case arises when the system is driven in such a way that $\Delta_o = -2\chi N_s$ which leads to $\Delta = 0$. In this case, the system remains stable and gives improved force sensitivity with a wider detection frequency range as compared to the case when $\Delta_o = \chi N_s = 0$ (as shown by the dashed curve in Fig. (4.1)).

In order to get further insight regarding the role of Kerr medium in the system, we have also calculated the intra-cavity photon number $N_s = |c_s|^2$ for three different cases as discussed in Fig. (4.1). The photon numbers obtained for case (i), (ii) and (iii) are 2.71×10^{11}, 2.13×10^{11} and 2.71×10^{11} respectively. For $\Delta = 0$, the photon number remains the same. However, for $\Delta \neq 0$, the intra-cavity photon number decreases in the presence of Kerr medium. Moreover, non-zero value of Δ

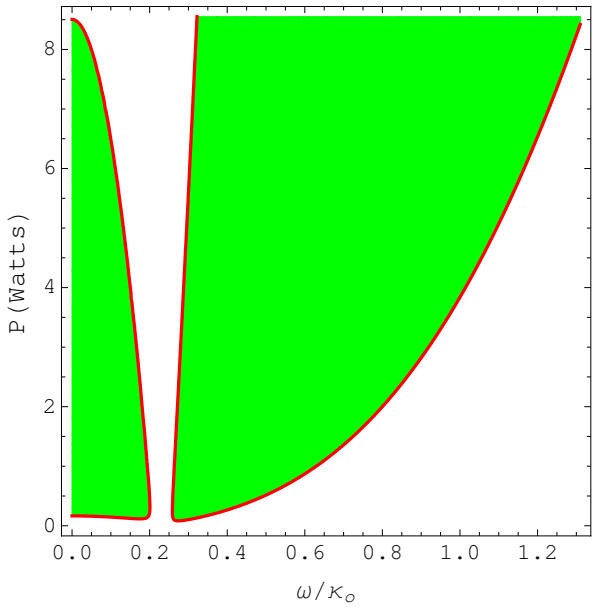

Figure 4.3: Contour plot of noise spectrum S_N against detection frequency ω/κ_o and input power P. Here we use $\Delta_o = -2\chi N_s = -0.3\kappa_o$. The solid line (in red color) represents S_N at SQL while the dark shaded region (in green color) is the region where S_N is below SQL.

also results in a slight shift in the oscillators resonance frequency which is evident from Fig. (4.1).

Figure (4.2) shows contour plots of S_N against detection frequency ω/κ_o and homodyne detection phase φ/π for the three cases as discussed in Fig. (4.1). Here all the contours are at SQL i.e., $S_N = 0$ dB. All the parameters are the same as in Fig. (4.1). Again we have dot-dashed contour for $\Delta_o = \chi N_s = 0$, solid contour for $\Delta_o = 0$, $\chi N_s/\kappa_o = 0.15$, and dashed contour for $\Delta_o = -2\chi N_s = -0.3\kappa_o$. The contours show that for each case there is a particular value of homodyne phase at which the range of detection frequency is maximum. For instance, the dot-dashed curve has maximum detection frequency range at $\varphi/\pi \approx -0.03$. For the solid contour the range is maximum for $\varphi/\pi \approx 0.035$ and for the dashed curve it is around $\varphi/\pi \approx 0.15$.

Figure (4.3) shows a contour plot of S_N against detection frequency ω/κ_o and input power P. Here we consider $\Delta_o = -2\chi N_s = -0.3\kappa_o$ i.e., $\Delta = 0$. The system remains stable under this condition as discussed earlier. The homodyne phase is set at $\varphi/\pi = 0.15$ while all the other parameters are the same as in Fig. (4.1). The solid contour (red line) is at SQL i.e. $S_N = 0$ dB while the dark shaded

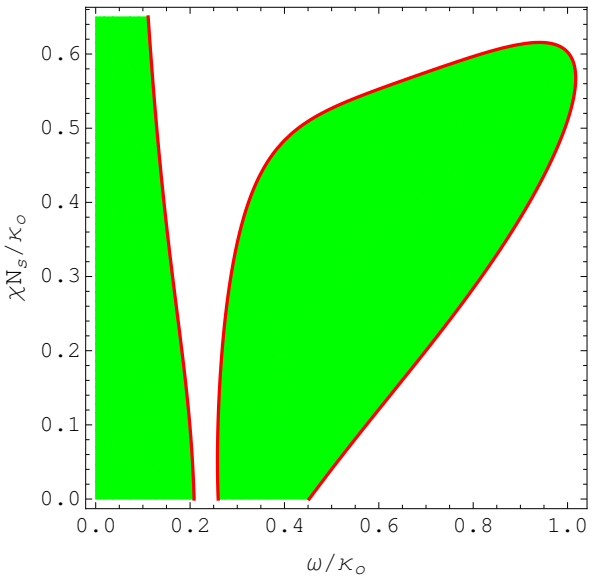

Figure 4.4: Contour plot of the noise spectrum S_N against ω/κ_o and $\chi N_s/\kappa_o$. The solid line (in red color) is at SQL i.e. $S_N = 0$ dB, while the dark shaded region (in green color) is the region where S_N is below SQL.

area (green color) corresponds to the region where the noise spectral density is below SQL. It is clear from Fig. (4.3), by increasing the input power, the range of detection frequency increases in the region where $\omega > \omega_m$ while there is a decrease in the range of detection frequency for $\omega < \omega_m$. The overall effect of high input power results in wider detection frequency range in the region where $\omega > \omega_m$.

Figure (4.4) shows the contour plot of the noise spectrum S_N against the detection frequency ω/κ_o and the strength of the Kerr non-linearity $\chi N_s/\kappa_o$. Here again we consider $\Delta_o = -2\chi N_s$ while the homodyne phase is set at $\varphi/\pi = 0.12$. All the other parameters are the same as in Fig. (4.1). The solid contour (red line) in Fig. (4.4) is at SQL while the dark shaded area (green color) represents the region where the noise spectral density is below SQL. Here we have two different choices for detection frequency (i) when the detection frequency is greater than the oscillator's frequency i.e., $\omega > \omega_m$ and (ii) when the detection frequency is smaller than the oscillator's frequency i.e., $\omega < \omega_m$. For $\omega > \omega_m$, maximum detection frequency range can be achieved for $0.35 < \chi N_s/\kappa_o < 0.5$ while for $\omega < \omega_m$ there is a slight decrease in the detection frequency range when the Kerr non-linearity is increased. Thus, an optimum choice of Kerr non-linearity is required in order to get large detection frequency range for below SQL sensitivity.

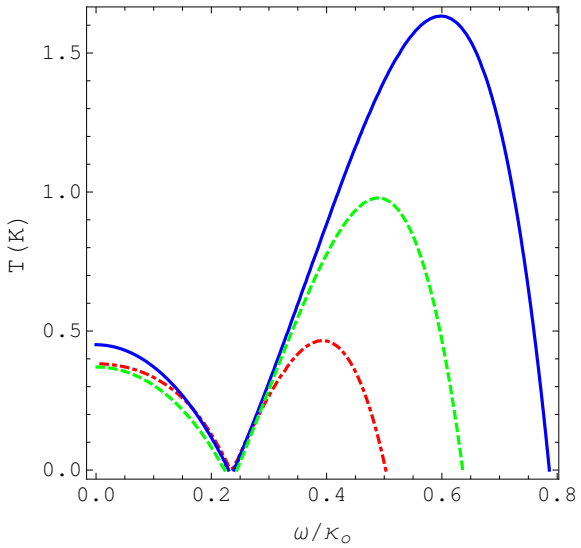

Figure 4.5: Contour plot of S_N against ω/κ_o and T for $\Delta_o = \chi N_s = 0$ (dot-dashed contour), $\Delta = \Delta_o + 2\chi N_s = 0$ (dashed contour) and for $\Delta_o = 0$, $\chi N_s/\kappa_o = 0.15$ (solid contour). All contours are at SQL i.e. at $S_N = 0$ dB. The solid and dashed contours show that the presence of Kerr media reduces the effects of temperature on force sensitivity. All the other parameters are the same as in fig. (4.1).

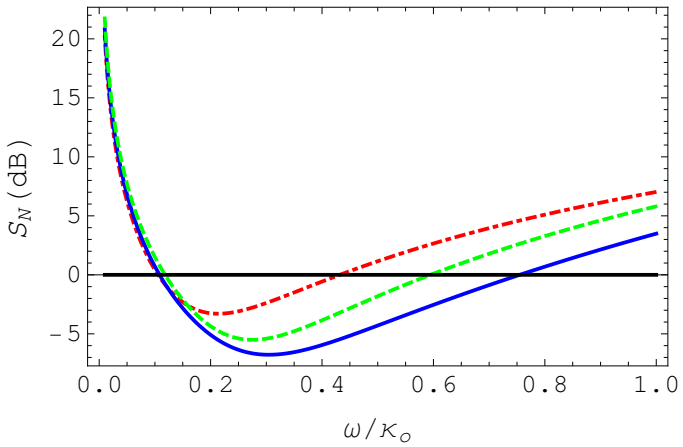

Figure 4.6: Noise spectrum S_N against the detection frequency ω/κ_o for $\Delta_o = \chi N_s = 0$ (dot-dashed contour), $\Delta_o = -2\chi N_s = 0.3\kappa_o$ (dashed contour) and for $\Delta_o = 0$, $\chi N_s/\kappa_o = 0.15$ (solid contour). Here we used $\omega_m/\kappa_o \approx 0$ and all the other parameters are the same as in fig. (4.1).

Next, we show how the temperature affects the force sensitivity of the oscillator. Consider Fig. (4.5) which shows a contour plot of S_N against ω/κ_o and T. All the contours are at SQL, i.e., at $S_N = 0$ dB. The dot-dashed, dashed and solid contours corresponds to $\Delta_o = \chi N_s = 0$, $\Delta = \Delta_o + 2\chi N_s = 0$ and $\Delta_o = 0$, $\chi N_s/\kappa_o = 0.15$, respectively. It is clear from dashed and solid contours in Fig. (4.5)

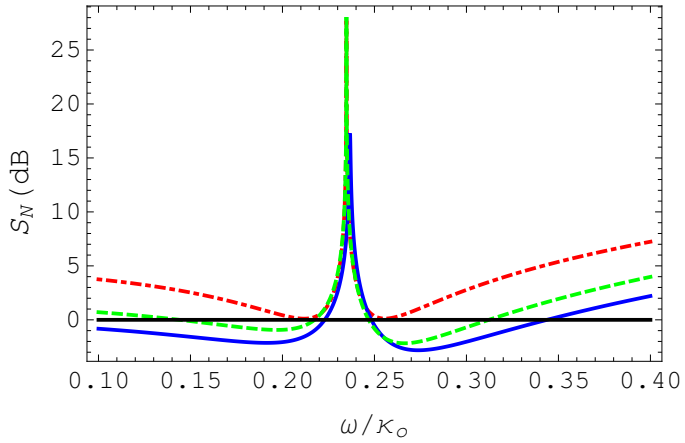

Figure 4.7: Noise spectrum S_N against the detection frequency ω/κ_o for $\Delta_o = \chi N_s = 0$ (dot-dashed curve), $\Delta_o = -2\chi N_s = 0.3\kappa_o$ (dashed curve) and for $\Delta_o = 0$, $\chi N_s/\kappa_o = 0.15$ (solid curve). Here we used $\gamma_m/\kappa_o \approx 10^{-7}$, $Q_m \approx 10^6$, $P = 100$ mW, $T = 5$ K and all the other parameters are the same as in fig. (4.1).

that the influence of temperature on force sensitivity is reduced in the presence of Kerr media which is quite interesting. Thus, the force sensitivity of the oscillator becomes more robust against the temperature in the presence of Kerr media.

Upto this point, we have discussed the force sensitivity of the mechanical oscillator. An interesting case arises when the frequency of mechanical oscillator is much smaller than the cavity line-width i.e. $\omega_m << \kappa_o$. Under this condition, the mechanical oscillator can be considered as a free mass. Figure (4.6) shows the noise spectrum of the free mass in the absence and presence of Kerr medium. The dot-dashed and solid curve represents the noise spectrum when the system is driven resonantly in the absence and presence of Kerr medium, respectively. The dashed curve represents the noise spectrum when both the Kerr medium and detuning are present such that $\Delta_o = -2\chi N_s = 0.3\kappa_o$. Figure (4.6) shows that force sensitivity is much better with a wider range of detection frequency in the presence of Kerr medium for a free test mass as well.

In Fig. (4.7),we have plotted the noise spectrum against the detection frequency for a different set of experimental parameters. The mechanical quality factor $Q_m \approx 10^6$ and mechanical damping $\gamma_m/\kappa_o \approx 10^{-7}$ [100,101]. Here the laser power is assumed to be $P = 100$ mW and the temperature $T = 5$ K. In the absence of Kerr medium, below SQL measurement is not possible as shown by the dot-dashed

curve. However, the presence of Kerr medium enables below SQL sensitivity as shown by the dashed and solid curve. It may be noted that quality factor in the range $10^7 - 10^9$ has already been reported for silicon-nitride membrane [100–102]. From experimental point of view, higher quality factor with low input power provide more flexibility on base temperature. Moreover, Kerr medium further enhances robustness against thermal noise.

4.4 Summary

To summarize the work presented in this chapter, we have considered the effects of Kerr medium in a dissipative OM system for force sensing of a mechanical oscillator. Our results show that the presence of the Kerr media improves the force sensitivity of the oscillator. The presence of Kerr media can also introduce system instability for some values of various parameters. However, the instability can be avoided if the system is driven by a blue detuned laser in such a way that $\Delta_o = -2\chi N_s$. If this condition is fulfilled, then there exist an optimum range of values for the Kerr non-linearity which leads to better force sensitivity below SQL with a wider range of detection frequency. Our results also show that by increasing the input power, force sensitivity and detection frequency range also increases. Moreover, the presence of Kerr media improves the robustness of the force sensitivity of the oscillator below the SQL against the thermal noise. It may also be noted that when frequency of the mechanical oscillator is much smaller than the cavity line-width i.e. $\Omega/\kappa_o \approx 0$, in this case the mechanical oscillator can be considered as a free mass. Our results show that better force sensitivity over a wide range of detection frequency can also be achieved for a free test mass in the presence of Kerr medium.

Chapter 5

Measurement of weak magnetic field via dissipatively coupled opto-mechanical system

5.1 Introduction

Optomechanical (OM) systems have proven its capability of providing potential applications in precision measurements. They can be used to achieve sensitivity beyond the standard quantum limit in gravitational wave detectors [18, 103–106], as a quantum speed meter [36, 39, 42], torque sensor [45], magnetometer [47, 48] and in precision measurement of electric charge [46].

In previous chapters, we discussed the detection of weak force signal via dissipative OM system. In this chapter, we present an optical detection technique for measuring weak magnetic field which can work at room temperature. We use a dissipatively coupled OM system that can be realized in a Michelson-Sagnac Interferometer (MSI) with a movable membrane [53–55]. MSI can be considered as a compound mirror as the position of the movable membrane sensitively affects the transmissivity of MSI when it operates close to the dark port condition. Under this condition, the compound MSI mirror along with a perfect mirror forms an effective Fabry-Perot Interferometer (FPI) whose linewidth depends upon the position of the membrane. In addition, when current is applied to the membrane in the presence of a magnetic field, it leads to the magnetic coupling of the membrane which directly affects the linewidth of the effective FPI. As a result, the output spectrum of the field is affected and therefore, enables measurement of weak magnetic field.

Rest of the chapter is organized as follows: In section 5.2, we present our model and solve the equations of motion. We find an expression for the output quadrature of the field and calculate the spectral density. In section 5.3, we present results of our numerical calculations. Finally, in section 5.4, we conclude our results.

5.2 Theory and Model

We consider an optomechanical system where a mechanical resonator of effective mass m and resonance frequency ω_m is dissipatively coupled to a cavity field with eigen-frequency ω_o. The cavity is driven with a strong coherent light of frequency $\omega_l = \omega_o$ and amplitude ε_l. In a frame rotating at input laser frequency ω_l, the Hamiltonian of the system is given by

$$\begin{aligned} \hat{H} &= \left(\frac{p^2}{2m} + \frac{1}{2}m\omega_m^2 x^2\right) + \hbar(\omega_o - \omega_l)c^\dagger c \\ &+ i\hbar\sqrt{2\kappa}[\varepsilon_l(c^\dagger - c) + c^\dagger c_{in} - c_{in}^\dagger c] + \zeta B x, \end{aligned} \tag{5.1}$$

where the first term describes the energy of the mechanical oscillator (MO) with x and p being the position and momentum operators satisfying the commutation relation $[x, p] = i\hbar$. The second term is the free energy of the cavity field. The third term represents the coupling of cavity field with the input laser and input vacuum noise represented by c_{in}. The last term represents the magnetic coupling of the MO where ζ is the current coefficient or magnetic coupling coefficient. It may also be noted that $\kappa = \kappa_o(1 + \eta x)$ represents the position dependent photon decay rate or half linewidth of the cavity and κ_o is the photon decay rate when $x = 0$. It is related to the dissipative coupling strength g_κ as $g_\kappa = x_{zpf} d\kappa/dx$ where $x_{zpf} = \sqrt{\hbar/2m\omega_m}$ is the zero point fluctuation of the membrane. Therefore, $g_\kappa = \eta\kappa_o x_{zpf}$ represents the dissipative coupling constant between the cavity field and MO which depends upon η. The parameter η is an experimental parameter and is related to the power reflectivity of the membrane and beam-splitter asymmetry [55]. The amplitude of the field is related to the input power $\mathbb{P}$ as $\varepsilon_l = \sqrt{\mathbb{P}/\hbar\omega_l}$.

The schematics of the system is shown in Fig. (5.1). It is assumed that the current is passing through the movable membrane M of MSI and the whole system

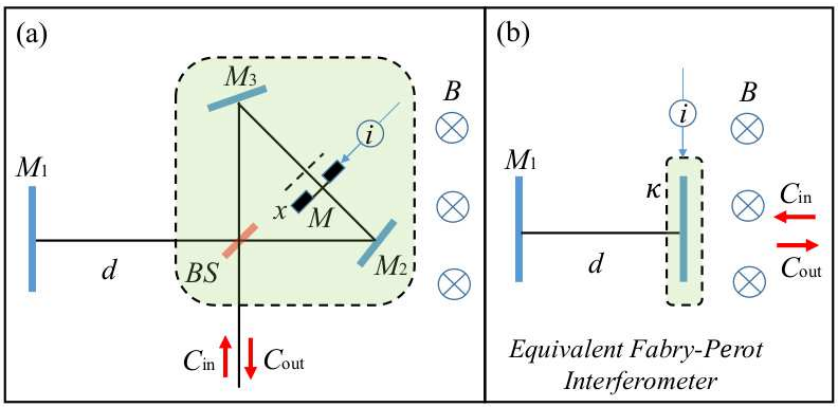

Figure 5.1: The schematics of the system. (a) A Michelson-Sagnac interferometer, containing the membrane M through which current i is flowing. The membrane is displaced from its mean position due to radiation pressure and external magnetic field B. (b) Equivalent Fabry-Perot interferometer whose right mirror have transmission depending upon the decay rate κ.

is placed in a magnetic field. The mean position of the membrane changes due to magnetic coupling of the membrane. The entire setup is equivalent to a Fabry-Perot Interferometer (FPI) with the variable optical decay rate i.e., $\kappa = \kappa_o(1+\eta x)$, where x is the displacement of the membrane. The displacement of the membrane can be controlled by the application of current in the presence of a magnetic field. Thus the right mirror of the effective FPI has an optical transmissivity that depends upon the current in the presence of magnetic field.

The Heisenberg equations of motion for the system when the cavity mode is resonantly pumped by the input laser (i.e., $\omega_o = \omega_l$) are given by the following:

$$\dot{x} = \frac{p}{m}, \tag{5.2a}$$

$$\dot{p} = -\frac{i\hbar\eta\sqrt{2\kappa_o}}{2}[\varepsilon_l(c^\dagger - c) + c^\dagger c_{in} - c_{in}^\dagger c] - m\omega_m^2 x - \zeta B - \gamma_m p + \xi, \tag{5.2b}$$

$$\dot{c} = \sqrt{2\kappa_o}(1 + \frac{\eta}{2}x)(\varepsilon_l + c_{in}) - \kappa_o(1+\eta x)c, \tag{5.2c}$$

where γ_m is the mechanical damping rate and ξ is the zero mean value thermal noise which describes the coupling of MO to the thermal environment. It follow immediately from Eqs. (5.2a)-(5.2c) that in steady-state, the position, momentum

and cavity field must fulfill the following self consistent equations:

$$p_s = 0,\ x_s = -\frac{\zeta B}{m\omega_m^2},\ c_s = \frac{\sqrt{2\kappa_o}(1+\eta x_s/2)\varepsilon_l}{\kappa_o(1+\eta x_s)}. \tag{5.3}$$

The operators given by Eqs. (5.2a)-(5.2c) can be represented as a sum of large mean value and small fluctuating terms such that $x = x_s + \delta x$, $p = p_s + \delta p$ and $c = c_s + \delta c$. In the first order approximation, the linearized equations of motion are given by

$$\delta\dot{x} = \frac{\delta p}{m}, \tag{5.4a}$$

$$\delta\dot{p} = -\frac{i\hbar\eta\sqrt{2\kappa_o}}{2}[\varepsilon_l(\delta c^\dagger - \delta c) + c_s(c_{in} - c_{in}^\dagger)] - m\omega_m^2\delta x - \gamma_m\delta p + \xi, \tag{5.4b}$$

$$\delta\dot{c} = -\kappa_o(1+\eta x_s)\delta c - \frac{\kappa_o\eta c_s}{2(1+\eta x_s/2)}\delta x + \sqrt{2\kappa_o}(1+\eta x_s/2)c_{in}. \tag{5.4c}$$

By taking the Fourier transform of Eqs. (5.4a)-(5.4c), the fluctuating position and cavity field in frequency domain can be written as:

$$\delta x(\omega) = \frac{1}{m[\omega_m^2 - \omega^2 - i\omega\gamma_m]}\left\{\xi - \frac{\hbar\eta\sqrt{2\kappa_o}\omega c_s}{2[\kappa_o(1+\eta x_s) - i\omega]}(c_{in} - c_{in}^\dagger)\right\}, \tag{5.5a}$$

$$\delta c(\omega) = \frac{1}{\kappa_o(1+\eta x_s/2) - i\omega}\left\{\sqrt{2\kappa_o}(1+\eta x_s/2)c_{in} - \frac{\kappa_o\eta c_s \times \delta x}{2(1+\eta x_s/2)}\right\}. \tag{5.5b}$$

By using Eqs. (5.5a) and (5.5b) and employing the input output relation (See Eq. (3.6b) in Chapter 3), the fluctuating output field of the system becomes:

$$\begin{aligned}\delta c_{out}(\omega) = &\left[\frac{2\kappa_o(1+\eta x_s/2)}{\kappa_o(1+\eta x_s) - i\omega} - 1\right]c_{in} \\ + &\left[1 - \frac{\kappa_o}{[\kappa_o(1+\eta x_s) - i\omega](1+\eta x_s/2)}\right]\frac{\sqrt{2\kappa_o}\eta c_s\delta x}{2}.\end{aligned} \tag{5.6}$$

As in the preceding chapters, we define the input amplitude and phase quadratures as $X_{in}(\omega) = \frac{1}{\sqrt{2}}[c_{in}(\omega) + c_{in}^\dagger(-\omega)]$ and $Y_{in}(\omega) = \frac{1}{i\sqrt{2}}[c_{in}(\omega) - c_{in}^\dagger(-\omega)]$. Similarly, the output field's amplitude and phase quadratures are defined as $X_{out}(\omega) = \frac{1}{\sqrt{2}}[\delta c_{out}(\omega) + \delta c_{out}^\dagger(-\omega)]$ and $Y_{out}(\omega) = \frac{1}{i\sqrt{2}}[\delta c_{out}(\omega) - \delta c_{out}^\dagger(-\omega)]$. On substituting the values of $\delta c_{out}(\omega)$ and $\delta c_{out}^\dagger(\omega)$, the output quadratures of the field are found

to be:

$$X_{out} = \frac{\kappa_o + i\omega}{\kappa_o(1+\eta x_s) - i\omega}\big[X_{in} + \alpha_1 Y_{in} - \alpha_2 \xi\big], \tag{5.7a}$$

$$Y_{out} = \frac{\kappa_o + i\omega}{\kappa_o(1+\eta x_s) - i\omega} Y_{in}, \tag{5.7b}$$

where α_1 and α_2 are defined as

$$\alpha_1 = \frac{iJ\kappa_o^2\chi\omega[\kappa_o - (1+\eta x_s/2)\{\kappa_o(1+\eta x_s) - i\omega\}]}{\omega_m(\kappa_o + i\omega)(1+\eta x_s/2)\{\kappa_o(1+\eta x_s) - i\omega\}}, \tag{5.8a}$$

$$\alpha_2 = \sqrt{\frac{J}{m\hbar}}\frac{\chi[\kappa_o - (1+\eta x_s/2)\{\kappa_o(1+\eta x_s) - i\omega\}]}{\omega_m(\kappa_o + i\omega)(1+\eta x_s/2)}, \tag{5.8b}$$

with $J = \hbar\eta^2 c_s^2/m\kappa_o$, being the dimensionless power and $\chi = \omega_m/(\omega_m^2 - \omega^2 - i\omega\gamma_m)$ is the mechanical susceptibility. The output field can also be expressed as $Z_{out}(\omega) = X_{out}(\omega)\cos\theta + Y_{out}(\omega)\sin\theta$, where θ represents the homodyne phase angle. On substituting Eqs. (5.7a) and (5.7b) in the generalized quadrature $Z_{out}(\omega)$, we obtained the following expression:

$$Z_{out}(\omega) \;=\; \frac{(\kappa_o + i\omega)\cos\theta}{\kappa_o(1+\eta x_s) - i\omega}\bigg[X_{in} + (\alpha_1 + \tan\theta)Y_{in} - \alpha_2\xi\bigg]. \tag{5.9}$$

Using Eq. (2.22), Eqs. (3.10a), (3.10b) and Eq. (3.11) of Chapter 2 and Chapter 3, the spectral density of the output field is found to be:

$$S_{out}(\omega) \;=\; \frac{(\kappa_o^2 + \omega^2)\cos^2\theta}{2[\kappa_o^2(1+\eta x_s)^2 + \omega^2]}\bigg[1 + |\alpha_1 + \tan\theta|^2 + 4mk_BT\gamma_m|\alpha_2|^2\bigg]. \tag{5.10}$$

In Eq. (5.10), the first term is the contribution from the photons shot noise, the second term is from the back-action and the last term is from the thermal noise. The homodyne phase angle θ can also be optimized to suppress the back action term. This can be done by setting the homodyne angle θ such that $\tan\theta_{opt} = -\alpha_1$.

5.3 Results and discussion

In this section, we present the results of our numerical simulation. Here, we consider $m = 50$ pg, $\kappa_o = 2\pi \times 59$ KHz, $\lambda = 1064$ nm, $g_k = 2\pi \times 2.6$ Hz, $Q = \omega_m/\gamma_m = 1.1 \times 10^7$, $T = 300$ K and $\omega_m \sim \kappa_o$ (i.e., non-resolved-sideband regime) as discussed in Ref. [54,107–109]. It may also be noted that SiN membrane

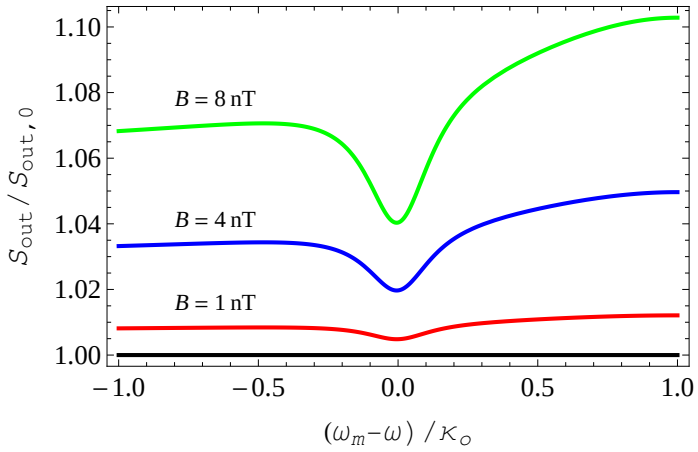

Figure 5.2: Normalized spectral density of the output field when $B = 0$ (straight line at $S_{out}/S_{out,0} = 1$), which becomes greater than 1 for $B \neq 0$. Here the parameters $m = 50$ pg, $\kappa_o = 2\pi \times 59$ KHz, $\lambda = 1064$ nm, $g_k = 2\pi \times 2.6$ Hz, $Q = \omega_m/\gamma_m = 1.1 \times 10^7$, $\omega_m \sim \kappa_o$, $P = 10$ μW, $T = 300$ K, $\zeta = 2 \times 10^{-5}$ A.m and $\omega_m/\kappa_o = 1$.

coated with Aluminium or Graphene [110, 111] can be used for the realization of current flowing through the membrane. As we discussed earlier, in the presence of magnetic field, the transmissivity of the right mirror of the effective FPI depends upon the current flowing through it. Therefore, a shift in the output spectral density of the field can be observed in the presence of magnetic field. Figure (5.2) shows the plot of normalized spectral density $S_{out}/S_{out,0}$ where $S_{out,0}$ represents the output field spectral density when B field is zero. Thus, $S_{out,0}$ represents the total noise floor. We also set the optimum homodyne angle at $\omega = \omega_m$ (i.e., substituting $\omega = \omega_m$ in $\tan\theta_{opt} = \alpha_1$) or equivalently when θ_{opt} is close to $\pi/2$ which leads to large dissipative coupling strength [63]. The input power $P = 10$ μW and the current flowing through the membrane is assumed to be $\zeta = 2 \times 10^{-5}$ A.m [48]. The solid straight line at $S_{out}/S_{out,0} = 1$ in Fig. (5.2) shows the normalized spectral density of the output field when B field is zero. When B field is turned on, the spectral density of the output field becomes greater than 1, i.e., $S_{out}/S_{out,0} > 1$ and the shift in the spectral density depends upon the strength of the magnetic field. The dip in the spectral density arises due to the membranes fundamental resonance. It may also be noted that shift in the spectral density is large when the detection frequency is smaller than the mechanical frequency as compared to

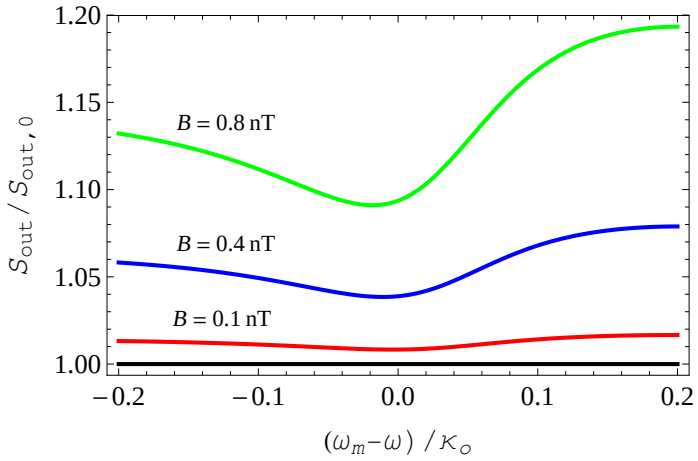

Figure 5.3: The plot shows that sub-nano-Tesla measurement can be made with better resolution if $\omega_m/\kappa_o < 1$. Here we used $\omega_m/\kappa_o = 0.2$, while all the other parameters are the same as in Fig. (5.2).

the case when the detection frequency is larger than the mechanical frequency. The system is relatively less sensitive to the magnetic field when the detection frequency is equal or close to the mechanical frequency.

It is interesting to note that, if we further shift towards the non-resolved-sideband regime for example, $\omega_m/\kappa_o = 0.2 < 1$ as in Ref. [43], the spectral density of the output field becomes more sensitive to the magnetic field as shown in Fig. (5.3). It may be pointed out that the micro- and nano-optomechanical devices due to their small size, inherently work in the bad cavity regime (i.e., $\omega_m/\kappa_o << 1$) [112], which is advantageous for our scheme. By comparing Fig. (5.2) and Fig. (5.3), it is clear that for $\omega_m/\kappa_o = 0.2$, shift in the output spectral density is larger even for the magnetic field strength ten times smaller than the results obtained for the case when $\omega_m/\kappa_o \sim 1$.

The measurement sensitivity can be further improved by adjusting the current flowing through the membrane. This is shown in Fig. (5.4), where the spectral density of the output field is plotted for three different choices of the current parameter ζ for $B = 0.1$ nT and $\omega_m/\kappa_o = 0.2$. Our results clearly show that the sensitivity of the measurement increases by increasing the current through the membrane. However, it may be pointed out that our analysis is based on linearization of the equations of motion around the large mean values (See Eqs. (5.4a)-(5.4c)), so for linear approximation to hold, current cannot be increased indefinitely. The linear

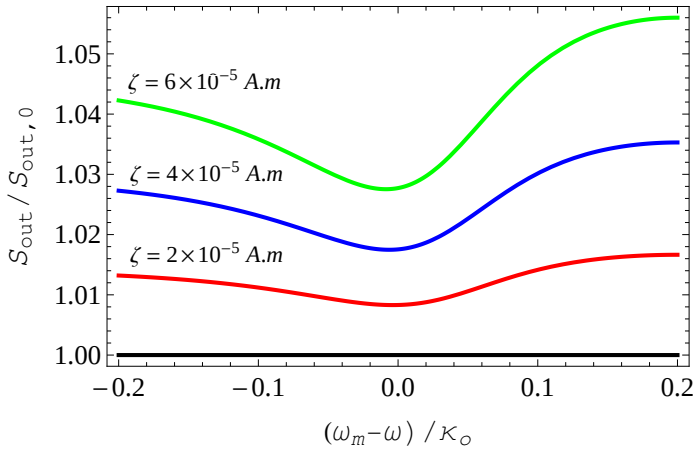

Figure 5.4: The spectral density of the output field for three different choices of current parameter ζ. Here $B = 0.1$ nT while all the other parameters are the same as in Fig. (5.3). By increasing the current, the spectral density shifts towards higher values, thus increasing the sensitivity of magnetic field (See Fig. (5.3) for a comparison).

approximation holds as long as $\eta x << 1$, so that the cavity linewidth κ is linearly related to the position x via $\kappa = \kappa_o(1 + \eta x)$. It is also interesting to note that, due to the topology of MSI, if the current is reversed i.e. $\zeta \to -\zeta$, the position of MO also shifts as $x \to -x$. Therefore, the Hamiltonian given by Eq. (5.1) is invariant under the transformation $\zeta \to -\zeta$ and $x \to -x$. As a result the output spectral density remains the same.

Figure (5.5) shows a contour plot of the output field spectral density with respect to the magnetic field and current at $\omega = \omega_m$ which is the resonance frequency of the membrane. At $\omega = \omega_m$, the shift in the spectral density is at its minimum (as can be seen in Figs. (5.2)-(5.4)). It is clear from Fig. (5.5) that for weak magnetic interaction (e.g., $B = 0.1$ nT and $\zeta = 2 \times 10^{-5}$ A.m), the shift in the output field spectral density is below 1.01 which can also be verified from Fig. (5.4) at $\omega = \omega_m$. The shift in the spectral density enhances when we increase the current or magnetic field. Thus, for an appropriate choice of current values, and detection frequency smaller than the mechanical frequency, and working in the non-resolved-side-band regime, B field upto sub-nano-Tesla levels can be measured by this scheme.

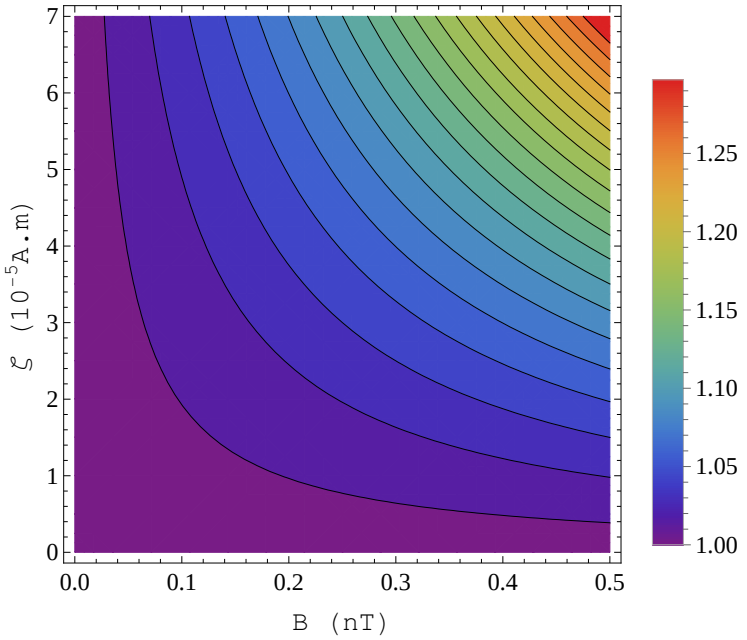

Figure 5.5: Contour plot of the normalized spectral density against B and ζ at $\omega_m = \omega$. Here $\omega_m/\kappa_o = 0.2$ and all the other parameters are the same as in Fig. (5.3).

5.4 Summary

In this chapter we considered a dissipative OM system for the detection of weak magnetic field. In the presence of magnetic field, the position of the membrane depends upon the current flowing through it. Thus by varying the current, the position of the membrane changes which leads to a change in the optical decay rate κ or transmissivity of the compound mirror. The effects of change in transmissivity can be seen in the output spectrum of the field. Therefore, by analyzing the spectrum of the output field, weak magnetic field can be measured. Our scheme is based on MSI which to the best of our knowledge is the only proven system for achieving pure dissipative coupling [54, 55]. From experimental point of view, dissipative coupling is more favorable in the micro- and nano-optomechanical devices. The optical line-width for such small devices typically scales inversely with the length of the cavity and eventually results in $\omega_m/\kappa_o << 1$, i.e., the so called non-resolved-sideband regime or bad cavity regime. Our proposal works better in this regime and therefore, could be more feasible to detect DC magnetic fields experimentally. Moreover, the system needs no magnetic shielding from the back-

ground, as measurements are made relative to the background. This also provides us the liberty to measure even weaker magnetic fields as long as the signal can be resolved from the background. Throughout our numerical simulations, we have used the parameters which are accessible in experiment. Therefore, we believe that our scheme enables potentially practical proposal for precision measurement of weak magnetic field. By adjusting the current and working in the non-resolved-side-band regime, one can make measurement of weak magnetic field upto sub-nano-Tesla levels at room temperature.

Chapter 6

Conclusion

In this thesis, we mainly focused on precision measurement using dissipatively coupled OM system. We theoretically investigated the effects of LPN associated with the laser that drives the OM cavity. In addition, we also studied the effects of LPN in the presence of PA with noisy pump laser. We also considered the effects of optical Kerr media on weak force measurement. Finally, we presented an optical detection technique for weak magnetic field measurement via dissipative coupling.

6.1 Summary

In Chapter 1, we have presented a brief introduction of optomechanics and its applications in precision measurement. We presented a brief review on dispersive and dissipative OM systems in the context of weak force measurement. The effect of LPN and Kerr medium in OM system were also briefly reviewed. A brief introduction on measurement of magnetic field via OM systems was also presented.

In Chapter 2, we have considered a dissipatively coupled OM system that can be used for force sensing below SQL for a free mass [42]. The laser that drives the OM system also has phase fluctuations which cannot be avoided completely due to its quantum nature. We introduced LPN into our system and studied its effects on free mass force sensing. Our analysis shows that the sensitivity of the force detection strongly depends upon the LPN. We also considered the effect of mechanical damping and thermal noise in the presence of phase fluctuations. The mechanical damping doesn't affect the force measurement substantially as long as $\gamma_m << \omega$, however, temperature greatly reduces the measurement sensitivity.

In the presence of laser phase fluctuation and thermal noise, the magnitude of input power of the laser also influences the force measurement sensitivity. Below SQL measurement can neither be achieved for very low power levels nor for very high power levels. Thus an optimum choice of various parameters involved in the system play an important role for force measurement in the presence of phase fluctuations, damping and thermal noise.

In Chapter 3, we have considered a dissipative OM system with PA which can also be used for free mass force sensing [43]. The presence of PA in the system results in further improvement of force sensing below SQL. However, the effects of LPN associated with the pump laser of PA were not considered. We therefore, introduced LPN associated with PA's pump and studied its effects on sensitivity of force measurement. We have not included the effects of LPN associated with the laser that drives the cavity because the noise bandwidth associated with the PA is much greater than the laser that drives the cavity due to the power broadening in PA pump [98]. Again, our results show that the sensitivity of the force detection strongly depends upon the laser phase fluctuation associated with the PA's pump. The presence of LPN limits the choice in the selection of various parameters for below SQL measurement. However, by suitably selecting various parameters, one can still achieve better than SQL sensitivity.

In Chapter 4, we have introduced an optical Kerr medium in a dissipative OM system and studied its effects on force sensing of a mechanical oscillator (MO). Our results show that the presence of Kerr medium not only improves the force sensitivity of MO below SQL but also makes the system more robust against thermal fluctuations. The presence of Kerr media can also introduce instability in the system for some values of various parameters. However, the instability can be avoided if the system is driven by a blue detuned laser such that $\Delta_o = -2\chi N_s$. Our results show that by increasing the input power, force sensitivity and detection frequency range also increase. In the limit $\omega_m << \kappa_o$, the MO can be considered as a free mass. Our results show that better force sensitivity over a wide range of detection frequency can also be achieved for a free test mass in the presence of Kerr medium.

Finally, in Chapter 5 we have presented an optical detection technique for the measurement of weak magnetic field based on dissipative OM system. For dissipative coupling, MSI with a movable membrane is considered which acts as a compound mirror having position dependent transmissivity. When current passes through the movable membrane in the presence of magnetic field, it leads to a change in the position of the membrane. Eventually, the transmissivity of the compound mirror changes and can be observed by the output spectrum of the field. Therefore, by analyzing the spectrum of the output field, weak magnetic field can be measured. The sensitivity of measurement can simply be controlled by the current passing through the membrane and working in the bad-cavity regime. Our proposal suggests measurement of weak magnetic field upto sub-nano-Tesla levels at room temperature. Thus, our scheme enables potentially practical proposal for precision measurement of weak magnetic field.

Appendix A

The parameters U, K, J, F_{SQL}, M_1, M_2 and M_3 in Eqs. (3.8a)-(3.8b) in Chapter 3 are defined as

$$U = \sqrt{\frac{16G^2+\omega^2}{(\kappa_o+2G)^2+\omega^2}}\frac{\kappa_o-i\omega+2G}{\omega+i4G}i, \tag{A.1}$$

$$K = J\frac{\kappa_o^2}{(\kappa_o+2G)^2+\omega^2}\frac{16G^2+\omega^2}{\omega^2}, \tag{A.2}$$

$$J = \frac{\hbar\eta^2 c_s^2}{m\kappa_o},\ F_{SQL}=\sqrt{2\hbar m\omega^2}, \tag{A.3}$$

$$M_1 = \frac{2c_sG\sqrt{\kappa_o}}{\omega(\kappa_o+i\omega+2G)}, \tag{A.4}$$

$$M_2 = \frac{iGKc_s(\kappa_o-2G)}{\sqrt{\kappa_o}\omega(4G-i\omega)}, \tag{A.5}$$

$$M_3 = \frac{2ic_sG\sqrt{\kappa_o}}{\omega(\kappa_o+i\omega-2G)}. \tag{A.6}$$

We also define the power parameter J by using the values of $c_s=\sqrt{2\kappa_o}\varepsilon_l(\kappa_o-2G)^{-1}$ and $\varepsilon_l=\sqrt{\mathbb{P}/\hbar\omega_l}$ as $J=J_o(1-2G/\kappa_o)^{-2}$, where $J_o=\frac{2\eta^2}{m\omega_l\kappa_o^2}\mathbb{P}$ refers to the power parameter in the absence of PA.

Appendix B

The parameters $h_1(\omega)$, $h_2(\omega)$, $h_3(\omega)$, $h_4(\omega)$, $h_5(\omega)$ and $h_6(\omega)$ in Eqs. (4.16a) and (4.16b) in Chapter 4 are defined as

$$\begin{aligned}
h_1(\omega) &= \sqrt{2\kappa_o}\Bigg[\frac{\sqrt{2\kappa_s}(b_1(\omega)+b_1^*(-\omega))}{a_2(\omega)} - 1 \\
&- Z_{eff}(\omega)a_5(\omega)\Big\{\frac{a_3(\omega)}{a_2(\omega)} + \frac{\eta(c_s+c_s^*)}{2\sqrt{2}}\Big\}\Bigg], \qquad \text{(B.1)} \\
h_2(\omega) &= \sqrt{2\kappa_o}\Bigg[\frac{-i\sqrt{2\kappa_s}(b_1(\omega)-b_1^*(-\omega))}{a_2(\omega)} \\
&+ Z_{eff}(\omega)a_6(\omega)\Big\{\frac{a_3(\omega)}{a_2(\omega)} + \frac{\eta(c_s+c_s^*)}{2\sqrt{2}}\Big\}\Bigg], \qquad \text{(B.2)} \\
h_3(\omega) &= \sqrt{2\kappa_o}\Bigg[Z_{eff}(\omega)\Big\{\frac{a_3(\omega)}{a_2(\omega)} + \frac{\eta(c_s+c_s^*)}{2\sqrt{2}}\Big\}\Bigg], \qquad \text{(B.3)} \\
h_4(\omega) &= i\sqrt{2\kappa_o}\Bigg[\frac{\sqrt{2\kappa_s}(a_1(\omega)-a_1^*(-\omega))}{a_2(\omega)} \\
&- Z_{eff}(\omega)a_5(\omega)\Big\{\frac{a_4(\omega)}{a_2(\omega)} - \frac{\eta(c_s-c_s^*)}{2\sqrt{2}}\Big\}\Bigg], \qquad \text{(B.4)} \\
h_5(\omega) &= \sqrt{2\kappa_o}\Bigg[iZ_{eff}(\omega)a_6(\omega)\Big\{\frac{a_4(\omega)}{a_2(\omega)} - \frac{\eta(c_s-c_s^*)}{2\sqrt{2}}\Big\} \\
&- \frac{\sqrt{2\kappa_s}(a_1(\omega)+a_1^*(-\omega))}{a_2(\omega)} - 1\Bigg], \qquad \text{(B.5)} \\
h_6(\omega) &= \sqrt{2\kappa_o}\Bigg[iZ_{eff}(\omega)\Big\{\frac{a_4(\omega)}{a_2(\omega)} - \frac{\eta(c_s-c_s^*)}{2\sqrt{2}}\Big\}\Bigg]. \qquad \text{(B.6)}
\end{aligned}$$

References

[1] J. C. Maxwell, *A treatise on electricity and magnetism.* Oxford, 1st ed., 1873.

[2] P. N. Lebedev, "Untersuchungen uber die druckkrafte des lichtes," *Annalen der Physik*, vol. 6, p. 433, 1901.

[3] E. F. Nichols and G. F. Hull, "A preliminary communication on the pressure of heat and light radiation," *Phys. Rev. (Series I)*, vol. 13, p. 307, 1901.

[4] M. Aspelmeyer, P. Meystre, and K. Schwab, "optomechanics," *Phys. Today*, vol. 65, p. 29, 2012.

[5] P. Meystre, "A short walk through quantum optomechanics," *Annalen der Physik*, vol. 525, p. 215, 2013.

[6] M. Aspelmeyer, T. J. Kippenberg, and F. Marquardt, "Cavity optomechanics," *Rev. Mod. Phys.*, vol. 86, p. 1391, 2014.

[7] F. Marquardt, J. P. Chen, A. A. Clerk, and S. M. Girvin, "Quantum theory of cavity-assisted sideband cooling of mechanical motion," *Phys. Rev. Lett.*, vol. 99, p. 093902, 2007.

[8] I. Wilson-Rae, N. Nooshi, W. Zwerger, and T. J. Kippenberg, "Theory of ground state cooling of a mechanical oscillator using dynamical backaction," *Phys. Rev. Lett.*, vol. 99, p. 093901, 2007.

[9] J. Chan, T. M. Alegre, A. H. Safavi-Naeini, J. T. Hill, A. Krause, S. Gröblacher, M. Aspelmeyer, and O. Painter, "Laser cooling of a nanome-

chanical oscillator into its quantum ground state," *Nature*, vol. 478, p. 89, 2011.

[10] J. D. Teufel, T. Donner, D. Li, J. W. Harlow, M. Allman, K. Cicak, A. J. Sirois, J. D. Whittaker, K. W. Lehnert, and R. W. Simmonds, "Sideband cooling of micromechanical motion to the quantum ground state," *Nature*, vol. 475, p. 359, 2011.

[11] S. Weis, R. Rivière, S. Deléglise, E. Gavartin, O. Arcizet, A. Schliesser, and T. J. Kippenberg, "Optomechanically induced transparency," *Science*, vol. 330, p. 1520, 2010.

[12] A. H. Safavi-Naeini, T. M. Alegre, J. Chan, M. Eichenfield, M. Winger, Q. Lin, J. T. Hill, D. E. Chang, and O. Painter, "Electromagnetically induced transparency and slow light with optomechanics," *Nature*, vol. 472, p. 69, 2011.

[13] D. E. Chang, A. H. Safavi-Naeini, M. Hafezi, and O. Painter, "Slowing and stopping light using an optomechanical crystal array," *New Journal of Physics*, vol. 13, p. 023003, 2011.

[14] K. Stannigel, P. Rabl, A. S. Sørensen, P. Zoller, and M. D. Lukin, "Optomechanical transducers for long-distance quantum communication," *Phys. Rev. Lett.*, vol. 105, p. 220501, 2010.

[15] C. A. Regal and K. W. Lehnert, "From cavity electromechanics to cavity optomechanics," *Journal of Physics: Conference Series*, vol. 264, p. 012025, 2011.

[16] T. A. Palomaki, J. W. Harlow, J. D. Teufel, R. W. Simmonds, and K. W. Lehnert, "Coherent state transfer between itinerant microwave fields and a mechanical oscillator," *Nature*, vol. 495, p. 210, 2013.

[17] M. J. Weaver, F. Buters, F. Luna, H. Eerkens, K. Heeck, S. de Man, and D. Bouwmeester, "Coherent optomechanical state transfer between disparate mechanical resonators," *Nature communications*, vol. 8, p. 1, 2017.

[18] J. Aasi, B. P. Abbott, *et al.*, "Advanced LIGO," *Classical and Quantum Gravity*, vol. 32, p. 074001, 2015.

[19] K. L. Dooley, T. Akutsu, S. Dwyer, and P. Puppo, "Status of advanced ground-based laser interferometers for gravitational-wave detection," *Journal of Physics: Conference Series*, vol. 610, p. 012012, 2015.

[20] B. P. Abbott *et al.*, "Observation of gravitational waves from a binary black hole merger," *Phys. Rev. Lett.*, vol. 116, p. 061102, 2016.

[21] I. Favero and F. Marquardt, "Focus on optomechanics," *New Journal of Physics*, vol. 16, p. 085006, 2014.

[22] M. Metcalfe, "Applications of cavity optomechanics," *Applied Physics Reviews*, vol. 1, p. 031105, 2014.

[23] D. Vitali, S. Gigan, A. Ferreira, H. R. Böhm, P. Tombesi, A. Guerreiro, V. Vedral, A. Zeilinger, and M. Aspelmeyer, "Optomechanical entanglement between a movable mirror and a cavity field," *Phys. Rev. Lett.*, vol. 98, p. 030405, 2007.

[24] T. A. Palomaki, J. D. Teufel, R. W. Simmonds, and K. W. Lehnert, "Entangling mechanical motion with microwave fields," *Science*, vol. 342, p. 710, 2013.

[25] V. B. Braginsky, A. B. Manukin, and G. M. Keiser, "Measurement of weak forces in physics experiments," *American Journal of Physics*, vol. 46, p. 195, 1978.

[26] C. M. Caves, "Quantum-mechanical radiation-pressure fluctuations in an interferometer," *Phys. Rev. Lett.*, vol. 45, p. 75, 1980.

[27] C. M. Caves, "Quantum-mechanical noise in an interferometer," *Phys. Rev. D*, vol. 23, p. 1693, 1981.

[28] A. F. Pace, M. J. Collett, and D. F. Walls, "Quantum limits in interferometric detection of gravitational radiation," *Phys. Rev. A*, vol. 47, p. 3173, 1993.

[29] V. B. Braginsky and F. Y. Khalili, "Quantum nondemolition measurements: the route from toys to tools," *Rev. Mod. Phys.*, vol. 68, p. 1, 1996.

[30] O. D. Aguiar, "Past, present and future of the resonant-mass gravitational wave detectors," *Research in Astronomy and Astrophysics*, vol. 11, p. 1, 2010.

[31] C. M. Caves, K. S. Thorne, R. W. P. Drever, V. D. Sandberg, and M. Zimmermann, "On the measurement of a weak classical force coupled to a quantum-mechanical oscillator. i. issues of principle," *Rev. Mod. Phys.*, vol. 52, p. 341, 1980.

[32] V. B. Braginsky and F. Y. Khalili, *Quantum measurement*. Cambridge University Press, 1992.

[33] J. D. Teufel, T. Donner, M. Castellanos-Beltran, J. W. Harlow, and K. W. Lehnert, "Nanomechanical motion measured with an imprecision below that at the standard quantum limit," *Nature nanotechnology*, vol. 4, p. 820, 2009.

[34] G. Anetsberger, E. Gavartin, O. Arcizet, Q. P. Unterreithmeier, E. M. Weig, M. L. Gorodetsky, J. P. Kotthaus, and T. J. Kippenberg, "Measuring nanomechanical motion with an imprecision below the standard quantum limit," *Phys. Rev. A*, vol. 82, p. 061804, 2010.

[35] U. B. Hoff, G. I. Harris, L. S. Madsen, H. Kerdoncuff, M. Lassen, B. M. Nielsen, W. P. Bowen, and U. L. Andersen, "Quantum-enhanced micromechanical displacement sensitivity," *Opt. Lett.*, vol. 38, p. 1413, 2013.

[36] V. B. Braginsky and F. Y. Khalili, "Gravitational wave antenna with QND speed meter," *Physics Letters A*, vol. 147, p. 251, 1990.

[37] V. Braginsky and F. Khalili, "Low noise rigidity in quantum measurements," *Physics Letters A*, vol. 257, p. 241, 1999.

[38] S. Vyatchanin and E. Zubova, "Quantum variation measurement of a force," *Physics Letters A*, vol. 201, p. 269, 1995.

[39] V. B. Braginsky, M. L. Gorodetsky, F. Y. Khalili, and K. S. Thorne, "Dual-resonator speed meter for a free test mass," *Phys. Rev. D*, vol. 61, p. 044002, 2000.

[40] H. J. Kimble, Y. Levin, A. B. Matsko, K. S. Thorne, and S. P. Vyatchanin, "Conversion of conventional gravitational-wave interferometers into quantum nondemolition interferometers by modifying their input and/or output optics," *Phys. Rev. D*, vol. 65, p. 022002, 2001.

[41] F. Khalili, "Frequency-dependent rigidity in large-scale interferometric gravitational-wave detectors," *Physics Letters A*, vol. 288, p. 251, 2001.

[42] S. P. Vyatchanin and A. B. Matsko, "Quantum speed meter based on dissipative coupling," *Phys. Rev. A*, vol. 93, p. 063817, 2016.

[43] S. Huang and G. S. Agarwal, "Robust force sensing for a free particle in a dissipative optomechanical system with a parametric amplifier," *Phys. Rev. A*, vol. 95, p. 023844, 2017.

[44] D. Mason, J. Chen, M. Rossi, Y. Tsaturyan, and A. Schliesser, "Continuous force and displacement measurement below the standard quantum limit," *Nature Physics*, vol. 15, p. 745, 2019.

[45] M. Wu, A. C. Hryciw, C. Healey, D. P. Lake, H. Jayakumar, M. R. Freeman, J. P. Davis, and P. E. Barclay, "Dissipative and dispersive optomechanics in a nanocavity torque sensor," *Phys. Rev. X*, vol. 4, p. 021052, 2014.

[46] J.-Q. Zhang, Y. Li, M. Feng, and Y. Xu, "Precision measurement of electrical charge with optomechanically induced transparency," *Phys. Rev. A*, vol. 86, p. 053806, 2012.

[47] S. Forstner, S. Prams, J. Knittel, E. D. van Ooijen, J. D. Swaim, G. I. Harris, A. Szorkovszky, W. P. Bowen, and H. Rubinsztein-Dunlop, "Cavity optomechanical magnetometer," *Phys. Rev. Lett.*, vol. 108, p. 120801, 2012.

[48] Z.-X. Liu, B. Wang, C. Kong, L.-G. Si, H. Xiong, and Y. Wu, "A proposed method to measure weak magnetic field based on a hybrid optomechanical system," *Scientific reports*, vol. 7, p. 1, 2017.

[49] B.-B. Li, J. Bílek, U. B. Hoff, L. S. Madsen, S. Forstner, V. Prakash, C. Schäfermeier, T. Gehring, W. P. Bowen, and U. L. Andersen, "Quantum enhanced optomechanical magnetometry," *Optica*, vol. 5, p. 850, 2018.

[50] W. Zhao, S.-D. Zhang, A. Miranowicz, and H. Jing, "Weak-force sensing with squeezed optomechanics," *Science China Physics, Mechanics & Astronomy*, vol. 63, p. 224211, 2019.

[51] R. S. Bondurant, "Reduction of radiation-pressure-induced fluctuations in interferometric gravity-wave detectors," *Phys. Rev. A*, vol. 34, p. 3927, 1986.

[52] Y. I. Vorontsov, "Uncertainty relation and the measurement error–perturbation relation," *Physics-Uspekhi*, vol. 48, p. 999, 2005.

[53] F. Elste, S. M. Girvin, and A. A. Clerk, "Quantum noise interference and backaction cooling in cavity nanomechanics," *Phys. Rev. Lett.*, vol. 102, p. 207209, 2009.

[54] A. Xuereb, R. Schnabel, and K. Hammerer, "Dissipative optomechanics in a michelson-sagnac interferometer," *Phys. Rev. Lett.*, vol. 107, p. 213604, 2011.

[55] A. Sawadsky, H. Kaufer, R. M. Nia, S. P. Tarabrin, F. Y. Khalili, K. Hammerer, and R. Schnabel, "Observation of generalized optomechanical coupling and cooling on cavity resonance," *Phys. Rev. Lett.*, vol. 114, p. 043601, 2015.

[56] T. Weiss and A. Nunnenkamp, "Quantum limit of laser cooling in dispersively and dissipatively coupled optomechanical systems," *Phys. Rev. A*, vol. 88, p. 023850, 2013.

[57] S. P. Tarabrin, H. Kaufer, F. Y. Khalili, R. Schnabel, and K. Hammerer, "Anomalous dynamic backaction in interferometers," *Phys. Rev. A*, vol. 88, p. 023809, 2013.

[58] M. Li, W. H. P. Pernice, and H. X. Tang, "Reactive cavity optical force on microdisk-coupled nanomechanical beam waveguides," *Phys. Rev. Lett.*, vol. 103, p. 223901, 2009.

[59] A. C. Hryciw, M. Wu, B. Khanaliloo, and P. E. Barclay, "Tuning of nanocavity optomechanical coupling using a near-field fiber probe," *Optica*, vol. 2, p. 491, 2015.

[60] T. Weiss, C. Bruder, and A. Nunnenkamp, "Strong-coupling effects in dissipatively coupled optomechanical systems," *New Journal of Physics*, vol. 15, p. 045017, 2013.

[61] G. S. Agarwal and S. Huang, "Electromagnetically induced transparency in mechanical effects of light," *Phys. Rev. A*, vol. 81, p. 041803, 2010.

[62] S. Huang and A. Chen, "Improving the cooling of a mechanical oscillator in a dissipative optomechanical system with an optical parametric amplifier," *Phys. Rev. A*, vol. 98, p. 063818, 2018.

[63] K. Qu and G. S. Agarwal, "Generating quadrature squeezed light with dissipative optomechanical coupling," *Phys. Rev. A*, vol. 91, p. 063815, 2015.

[64] D. Kilda and A. Nunnenkamp, "Squeezed light and correlated photons from dissipatively coupled optomechanical systems," *Journal of Optics*, vol. 18, p. 014007, 2015.

[65] A. K. Tagantsev, I. V. Sokolov, and E. S. Polzik, "Dissipative versus dispersive coupling in quantum optomechanics: Squeezing ability and stability," *Phys. Rev. A*, vol. 97, p. 063820, 2018.

[66] S. Qamar, H. Xiong, and M. S. Zubairy, "Influence of pump-phase fluctuations on entanglement generation using a correlated spontaneous-emission laser," *Phys. Rev. A*, vol. 75, p. 062305, 2007.

[67] S. Qamar, S. Qamar, and M. S. Zubairy, "Effect of phase fluctuations on entanglement generation in a correlated emission laser with injected coherence," *Optics Communications*, vol. 283, p. 781, 2010.

[68] G. A. Phelps and P. Meystre, "Laser phase noise effects on the dynamics of optomechanical resonators," *Phys. Rev. A*, vol. 83, p. 063838, 2011.

[69] M. Abdi, S. Barzanjeh, P. Tombesi, and D. Vitali, "Effect of phase noise on the generation of stationary entanglement in cavity optomechanics," *Phys. Rev. A*, vol. 84, p. 032325, 2011.

[70] R. Ghobadi, A. R. Bahrampour, and C. Simon, "Optomechanical entanglement in the presence of laser phase noise," *Phys. Rev. A*, vol. 84, p. 063827, 2011.

[71] L. Mandel and E. Wolf, *Optical coherence and quantum optics*. NewYork: Cambridge university press, 1995.

[72] H. Haken, *Laser theory*. Springer-Verlag, 1984.

[73] L. Diósi, "Laser linewidth hazard in optomechanical cooling," *Phys. Rev. A*, vol. 78, p. 021801, 2008.

[74] P. Rabl, C. Genes, K. Hammerer, and M. Aspelmeyer, "Phase-noise induced limitations on cooling and coherent evolution in optomechanical systems," *Phys. Rev. A*, vol. 80, p. 063819, 2009.

[75] A. Mehmood, S. Qamar, and S. Qamar, "Effects of laser phase fluctuation on force sensing for a free particle in a dissipative optomechanical system," *Phys. Rev. A*, vol. 98, p. 053841, 2018.

[76] A. Mehmood, S. Qamar, and S. Qamar, "Force sensing in a dissipative optomechanical system in the presence of parametric amplifier's pump phase noise," *Physica Scripta*, vol. 94, p. 095502, 2019.

[77] H.-H. Ritze and A. Bandilla, "Quantum effects of a nonlinear interferometer with a kerr cell," *Optics Communications*, vol. 29, p. 126, 1979.

[78] H.-H. Ritze and A. Bandilla, "A new proposal for measuring the quantum fluctuations in a light beam using a nonlinear interferometer," *Optics Communications*, vol. 30, p. 125, 1979.

[79] N. Imoto, H. A. Haus, and Y. Yamamoto, "Quantum nondemolition measurement of the photon number via the optical kerr effect," *Phys. Rev. A*, vol. 32, p. 2287, 1985.

[80] T. Kumar, A. B. Bhattacherjee, and ManMohan, "Dynamics of a movable micromirror in a nonlinear optical cavity," *Phys. Rev. A*, vol. 81, p. 013835, 2010.

[81] D. Zhang, X.-P. Zhang, and Q. Zheng, "Enhancing stationary optomechanical entanglement with the kerr medium," *Chinese Physics B*, vol. 22, p. 064206, 2013.

[82] A. A. Nejad, H. R. Askari, and H. R. Baghshahi, "Bistability in a hybrid optomechanical system under the effect of a nonlinear medium," *Chinese Physics Letters*, vol. 34, p. 084205, 2017.

[83] A. B. Bhattacherjee and M. S. Hasan, "Controllable optical bistability and fano line shape in a hybrid optomechanical system assisted by kerr medium: possibility of all optical switching," *Journal of Modern Optics*, vol. 65, p. 1688, 2018.

[84] A. Edelstein, "Advances in magnetometry," *Journal of Physics: Condensed Matter*, vol. 19, p. 165217, 2007.

[85] M. V. Romalis and H. B. Dang, "Atomic magnetometers for materials characterization," *Materials Today*, vol. 14, p. 258, 2011.

[86] F. Bucholtz, D. M. Dagenais, and K. P. Koo, "High-frequency fibre-optic magnetometer with 70 ft/ square root (hz) resolution," *Electronics Letters*, vol. 25, p. 1719, 1989.

[87] J. Zhai, Z. Xing, S. Dong, J. Li, and D. Viehland, "Detection of pico-tesla magnetic fields using magneto-electric sensors at room temperature," *Applied Physics Letters*, vol. 88, p. 062510, 2006.

[88] H. B. Dang, A. C. Maloof, and M. V. Romalis, "Ultrahigh sensitivity magnetic field and magnetization measurements with an atomic magnetometer," *Applied Physics Letters*, vol. 97, p. 151110, 2010.

[89] W. Wasilewski, K. Jensen, H. Krauter, J. J. Renema, M. V. Balabas, and E. S. Polzik, "Quantum noise limited and entanglement-assisted magnetometry," *Phys. Rev. Lett.*, vol. 104, p. 133601, 2010.

[90] D. F. Walls and G. J. Milburn, *Quantum optics*. Springer-Verlag Berlin Heidelberg, 1st ed., 1994.

[91] S. Huang and G. S. Agarwal, "Reactive-coupling-induced normal mode splittings in microdisk resonators coupled to waveguides," *Phys. Rev. A*, vol. 81, p. 053810, 2010.

[92] A. A. Clerk, M. H. Devoret, S. M. Girvin, F. Marquardt, and R. J. Schoelkopf, "Introduction to quantum noise, measurement, and amplification," *Rev. Mod. Phys.*, vol. 82, p. 1155, 2010.

[93] U. L. Andersen, T. Gehring, C. Marquardt, and G. Leuchs, "30 years of squeezed light generation," *Physica Scripta*, vol. 91, p. 053001, 2016.

[94] S. Sakata, S. Kawamura, S. Sato, K. Somiya, K. Arai, M. Fukushima, and A. Sugamoto, "Development of a control scheme of homodyne detection for extracting ponderomotive squeezing from a michelson interferometer," *Journal of Physics: Conference Series*, vol. 32, p. 464, 2006.

[95] E. Oelker, G. Mansell, M. Tse, J. Miller, F. Matichard, L. Barsotti, P. Fritschel, D. E. McClelland, M. Evans, and N. Mavalvala, "Ultra-low phase noise squeezed vacuum source for gravitational wave detectors," *Optica*, vol. 3, p. 682, 2016.

[96] Y. Takeno, M. Yukawa, H. Yonezawa, and A. Furusawa, "Observation of -9 db quadrature squeezing with improvement of phase stability in homodyne measurement," *Opt. Express*, vol. 15, p. 4321, 2007.

[97] R. Schnabel, "Squeezed states of light and their applications in laser interferometers," *Physics Reports*, vol. 684, p. 1, 2017. Squeezed states of light and their applications in laser interferometers.

[98] F. Farman and A. R. Bahrampour, "Effects of optical parametric amplifier pump phase noise on the cooling of optomechanical resonators," *J. Opt. Soc. Am. B*, vol. 30, p. 1898, 2013.

[99] E. X. DeJesus and C. Kaufman, "Routh-hurwitz criterion in the examination of eigenvalues of a system of nonlinear ordinary differential equations," *Phys. Rev. A*, vol. 35, p. 5288, 1987.

[100] T. P. Purdy, R. W. Peterson, P.-L. Yu, and C. A. Regal, "Cavity optomechanics with si3n4membranes at cryogenic temperatures," *New Journal of Physics*, vol. 14, p. 115021, 2012.

[101] R. Fischer, D. P. McNally, C. Reetz, G. G. T. Assumpção, T. Knief, Y. Lin, and C. A. Regal, "Spin detection with a micromechanical trampoline: towards magnetic resonance microscopy harnessing cavity optomechanics," *New Journal of Physics*, vol. 21, p. 043049, 2019.

[102] M. Rossi, D. Mason, J. Chen, Y. Tsaturyan, and A. Schliesser, "Measurement-based quantum control of mechanical motion," *Nature*, vol. 563, p. 53, 2018.

[103] V. B. Braginski and A. B. Manukin, "Ponderomotive effects of electromagnetic radiation," *Sov. Phys. JETP*, vol. 25, p. 653, 1967.

[104] V. B. Braginski and A. B. Manukin, "Investigation of dissipative ponderomotive effects of electromagnetic radiation," *JETP*, vol. 31, p. 829, 1970.

[105] V. B. Braginsky, M. L. Gorodetsky, and F. Y. Khalili, "Optical bars in gravitational wave antennas," *Physics Letters A*, vol. 232, p. 340, 1997.

[106] A. Buonanno and Y. Chen, "Signal recycled laser-interferometer gravitational-wave detectors as optical springs," *Phys. Rev. D*, vol. 65, p. 042001, 2002.

[107] J. D. Thompson, B. Zwickl, A. Jayich, F. Marquardt, S. Girvin, and J. Harris, "Strong dispersive coupling of a high-finesse cavity to a micromechanical membrane," *Nature*, vol. 452, no. 7183, p. 72, 2008.

[108] B. M. Zwickl, W. E. Shanks, A. M. Jayich, C. Yang, A. C. Bleszynski Jayich, J. D. Thompson, and J. G. E. Harris, "High quality mechanical and optical properties of commercial silicon nitride membranes," *Applied Physics Letters*, vol. 92, p. 103125, 2008.

[109] U. Kemiktarak, M. Metcalfe, M. Durand, and J. Lawall, "Mechanically compliant grating reflectors for optomechanics," *Applied Physics Letters*, vol. 100, p. 061124, 2012.

[110] T. Bagci, A. Simonsen, S. Schmid, L. Villanueva Torrijo, E. Zeuthen, J. Appel, J. Taylor, A. Sørensen, K. Usami, A. Schliesser, and E. Polzik, "Optical detection of radio waves through a nanomechanical transducer.," *Nature*, vol. 507, p. 81, 2014.

[111] S. Schmid, T. Bagci, E. Zeuthen, J. M. Taylor, P. K. Herring, M. C. Cassidy, C. M. Marcus, L. Guillermo Villanueva, B. Amato, A. Boisen, Y. Cheol Shin, J. Kong, A. S. Sørensen, K. Usami, and E. S. Polzik, "Single-layer graphene on silicon nitride micromembrane resonators," *Journal of Applied Physics*, vol. 115, p. 054513, 2014.

[112] J. S. Bennett, K. Khosla, L. S. Madsen, M. R. Vanner, H. Rubinsztein-Dunlop, and W. P. Bowen, "A quantum optomechanical interface beyond the resolved sideband limit," *New Journal of Physics*, vol. 18, p. 053030, 2016.